NASA TECHNICAL NOTE

NASA TN D-2462

c. 1

LOAN

TECH LIBRARY KAFB, NM

0079557

NASA TN D-2462

WIND-TUNNEL MEASUREMENTS ON A LIFTING ROTOR AT HIGH THRUST COEFFICIENTS AND HIGH TIP-SPEED RATIOS

by George E. Sweet, Julian L. Jenkins, Jr., and Matthew M. Winston

Langley Research Center
Langley Station, Hampton, Va.

NATIONAL AERONAUTICS AND SPACE ADMINISTRATION • WASHINGTON, D. C. • SEPTEMBER 1964

TECH LIBRARY KAFB, NM

0079557

WIND-TUNNEL MEASUREMENTS ON A LIFTING ROTOR AT HIGH THRUST COEFFICIENTS AND HIGH TIP-SPEED RATIOS

By George E. Sweet, Julian L. Jenkins, Jr., and Matthew M. Winston

Langley Research Center
Langley Station, Hampton, Va.

NATIONAL AERONAUTICS AND SPACE ADMINISTRATION

For sale by the Office of Technical Services, Department of Commerce,
Washington, D.C. 20230 -- Price $1.50

WIND-TUNNEL MEASUREMENTS ON A LIFTING ROTOR AT HIGH THRUST COEFFICIENTS AND HIGH TIP-SPEED RATIOS

By George E. Sweet, Julian L. Jenkins, Jr.,
and Matthew M. Winston
Langley Research Center

SUMMARY

Results are presented from an investigation of the performance and static stability characteristics of a 15-foot-diameter rotor operating at conditions expected to produce large amounts of blade stall.

Rotor forces, power, and flapping motions were recorded for rotor tip-path-plane angles of attack of 10.5°, 0.5°, and -9.5° at tip-speed ratios from 0.25 to 0.56. Portions of the data are compared with theoretical calculations.

At theoretically unstalled operating conditions, the agreement between measured and calculated rotor thrust was good. However, when rotor-blade stall was theoretically predicted, thrust measurements did not indicate the large blade lift losses predicted by theory. The measured profile power was significantly greater than calculated for conditions in which no stall was expected. The longitudinal rotor flapping did not show any sudden divergence when stall was encountered. The rotor exhibited stabilizing trends for large changes in angle of attack.

INTRODUCTION

Although rotary-wing aircraft are normally designed to cruise under conditions in which little or no rotor-blade stall is present, large portions of the rotor may stall during maneuvers, in gusty air, or in high-speed flight. Future development of high-performance rotary-wing aircraft with an all-weather capability depends upon a knowledge of the effects of blade stall on rotor operation. Because of the complexities involved in experimentally determining the effects of blade stall on rotor-fuselage clearances, control requirements, static stability, and performance, analytical procedures are desired. However, the applicability of analytical approaches is still largely unverified for conditions involving large amounts of blade stall and at high tip-speed ratios.

Recently, wind-tunnel tests were conducted at the Langley Research Center with a 15-foot-diameter rotor operating at conditions expected to produce large areas of blade stall. The purpose of these tests was to provide a basis for further experimental and analytical study of the effects of blade stall and/or high tip-speed ratios on rotor aerodynamics and blade motions.

Measurements of rotor forces, power, and flapping and feathering motions were made for several thrust coefficients at tip-speed ratios from 0.25 to 0.56 for tip-path-plane angles of attack of 10.5°, 0.5°, and -9.5°. Tests were also made to determine static-stability derivatives with respect to velocity, and the effects of large shaft-angle changes on rotor aerodynamics were investigated.

Representative portions of the test data are compared with calculations based on simple and refined blade-element theories. Photographs of tufts attached to the rotor blades were made to aid in interpretations of these comparisons.

A preliminary interpretation of a portion of these results is presented in reference 1.

SYMBOLS

The positive directions of forces and angles are shown in figure 1.

A_o blade collective pitch angle; angle between line of zero lift of blade section and plane perpendicular to axis of no feathering, deg

a' angle between control axis and resultant-force vector in longitudinal plane, deg

a_1 coefficient of $-\cos\psi$ in expression for β; hence, longitudinal tilt of rotor cone, positive for rearward tilt, deg

b number of blades

b_1 coefficient of $-\sin\psi$ in expression for β; hence, lateral tilt of rotor cone, positive for tilt toward advancing side, deg

C_H rotor in-plane drag (H force) coefficient, $\dfrac{H}{\pi R^2 \rho (\Omega R)^2}$

$\bar{C}_L$ equivalent hovering mean-lift coefficient, $\dfrac{6C_T}{\sigma}$

C_P power coefficient, $\dfrac{P}{\pi R^2 \rho (\Omega R)^3}$

C_R rotor resultant-force coefficient

C_T rotor thrust coefficient, $\frac{T}{\pi R^2 \rho (\Omega R)^2}$

C_Y rotor side-force coefficient, $\frac{Y}{\pi R^2 \rho (\Omega R)^2}$

c blade section chord, ft

f equivalent parasite-drag area, sq ft

H longitudinal component of rotor resultant force perpendicular to shaft axis, lb

$\left(\frac{L}{D}\right)_r$ equivalent rotor lift-drag ratio, $\frac{C_T}{C_P - C_{P,p}} \frac{V}{\Omega R}$

N_{Re} Reynolds number, $\frac{\Omega R c}{\nu}$ or $\frac{Vc}{\nu}$

P power, ft-lb/sec

R rotor radius, ft

T rotor thrust, lb

V free-stream velocity, ft/sec

Y rotor side force, lb

α section angle of attack, deg

α_{Tip} section angle of attack at rotor tip, deg

α_s rotor-shaft angle of attack, deg

α_{TPP} rotor tip-path-plane angle of attack; angle between flight path and plane perpendicular to axis of no flapping, deg

β blade flapping angle at particular azimuth position ($\beta = -a_1 \cos \psi - b_1 \sin \psi \ . \ . \ .$), deg

ν kinematic viscosity

ρ mass density of air, slugs/cu ft

σ rotor solidity, $bc/\pi R$

ψ blade azimuth angle measured from rearmost point of rotor in direction of rotation, deg

Ω rotor angular velocity, radians/sec

Subscripts:

i induced

o profile

p parasite

s referenced to shaft axis

APPARATUS

The rotor apparatus and photographic equipment as installed in the Langley full-scale tunnel are shown in figure 2. A large ground-reflection plane was installed below the rotor to minimize the problem of jet-boundary corrections.

Rotor

The test rotor was of a two-blade teetering type with no built-in coning. The rotor was 15.25 feet in diameter with a constant chord of 1.16 feet and a solidity of 0.0968. The blades were untwisted NACA 0012 airfoil sections. A 0.25-inch strip of No. 60 carborundum grains (0.012-inch mean grain diameter) was sparsely distributed along the blade span on the upper surface at the 10-percent chord station. Its purpose was to avoid variations in section characteristics by fixing the transition point. It is believed that the primary effect of this strip was to increase the profile drag to a value that is representative of production-line blades in normal use. The blade stiffness both in bending and in torsion was large in relation to the rotor loads; therefore, periodic twist due to airloads is believed to have been small.

Instrumentation

Rotor thrust and torque were measured by strain-gage instrumentation located within the rotor-support tower (fig. 3). This apparatus automatically corrected for thrust loads carried by the blade-pitch-change rods and for the friction torque of the swash plate; consequently, the true rotor thrust and torque were recorded. The total drag of the model was measured with a mechanical balance. Rotor longitudinal force was obtained by subtracting tares taken with the blades removed from the rotor-operating data. Blade flapping and feathering motions were sensed by strain gages and recorded on an oscillograph. A Fourier analysis was performed on these data to determine the first harmonic flapping and feathering coefficients. Rotor rotational speed was sensed by a magnetic pickup and recorded on an oscillograph.

The overall accuracies of the data are believed to be within the following limits:

C_T	±0.00025
C_H	±0.00015
C_Y	±0.00020
C_P	±0.00002
Rotor tip speed, ft/sec	±1
Rotor tip-speed ratio	±0.01
Shaft angle of attack, collective pitch, lateral cyclic pitch, and flapping motions, deg	±0.25
Longitudinal cyclic pitch, deg	±0.50

Tuft Photographs

Multiexposure photographs of tufts attached to the rotor blades were made with the camera and flash equipment shown in figure 2. During one rotor revolution, five exposures, spaced at intervals of about 40° in azimuth on the retreating side of the rotor disk, were made. An additional five exposures, at intermediate azimuth positions, were made about 1 minute after the first photographs.

TESTS AND CORRECTIONS

All tests were run at a rotor tip speed of about 215 feet per second which corresponds to a hovering tip Reynolds number N_{Re} of about 1.6×10^6.

Performance measurements were made at rotor tip-path-plane angles of attack of -9.5°, 0.5°, and 10.5° with the tip-path plane trimmed normal to the shaft for all thrust settings. This range includes negative power conditions not normally encountered in helicopter flight. Several of these tests were repeated with tufts attached to the blades for the purpose of obtaining photographic data.

Measurements to determine the static-stability characteristics of the rotor were made for independent changes in velocity and shaft angle of attack with the rotor controls fixed. The initial trim condition was taken as the case where the tip-path plane was normal to the shaft axis.

The velocity changes were small (from 4 to 6 feet per second) so that static-stability derivatives could be determined; however, the angle-of-attack increments were large, and only the gross effects of angle-of-attack changes were determined.

A stream-angle correction of 0.5° was applied to all data. No jet-boundary corrections were applied; with the tunnel configurations used, they should be negligible for the present range of test conditions (ref. 2).

METHOD OF ANALYSIS

The two types of calculations (simple and refined) that are compared with the measured data are based on blade-element theory with uniform inflow assumed. Measured tip-speed ratio, collective pitch, and longitudinal and lateral cyclic pitch were used in the calculations. The theoretical inflow ratio was varied until the calculated angle of attack of the tip-path plane matched the measured angle within $\pm 0.35^{\circ}$.

Simple Theory

The simple-theory calculations are based on the blade-element theory presented in reference 3. A constant lift-curve slope of 5.55 per radian was used (ref. 4). Rather than use a constant mean-rotor-drag coefficient, the changes in the mean value due to lift and forward velocity were estimated by use of the following equation (ref. 5):

$$\delta = \delta_o\left\{1 + \frac{36C_T^{\,2}}{\sigma^2\left[1 + 7.5\left(\frac{V}{\Omega R}\right)^2\right]}\right\}$$

where the zero-lift profile-drag coefficient δ_o was determined to be 0.0087 from preliminary hovering tests of this rotor. Rotor flapping coefficients were determined by the method of reference 6. Effects of stall, tip losses, blade cutout, and the reversed velocities were not accounted for in the simple calculations.

Refined Theory

The refined calculations were carried out on a high-speed, electronic data processing machine, which was programed according to the equations presented in references 7 and 8. These equations account for stall, tip losses, blade cutout, and the reversed-velocity region. The blade-section characteristics used are compared with two-dimensional section characteristics of the NACA 0012 airfoil section (ref. 9) in figure 4. It is believed that the differences between the measured section characteristics and those used in the calculations are within the range of applicability of steady-state, two-dimensional data to the present rotor calculations. The point at which blade-tip stall is predicted $\left(\alpha_{Tip} > 12^{\circ}\right)$ is indicated in the refined-theory curves.

Static-Stability Derivatives

The measurements for determining static stability were first plotted against the independent variable, velocity. The slope through the initial trim values was then measured to obtain the derivative. The calculated derivatives were obtained in a similar manner from the calculated slopes.

PRESENTATION OF RESULTS

The results of this investigation are presented in the following order:

	Figure
Measured rotor characteristics:	
Total rotor power	5
Rotor drag force	6
Rotor side force	7
Equivalent rotor flapping coefficients	8
Collective pitch	9
Equivalent parasite drag	10
Equivalent rotor lift-drag ratio	11
Plots of measured and calculated performance against tip-speed ratio for measured thrust coefficients of 0.0035 and 0.0070:	
$\alpha_{TPP} = 10.5^{\circ}$	12
$\alpha_{TPP} = 0.5^{\circ}$	13
$\alpha_{TPP} = -9.5^{\circ}$	14
Plots of ratios of measured thrust to calculated thrust against $\overline{C}_L$ and plots of ratios of measured profile power to calculated profile power against $\overline{C}_L$	15
Measured and calculated longitudinal flapping coefficients	16
Changes in tuft flow patterns with increases in lift	17
Overlays of contours of constant section angle of attack on tuft photographs	18
Summary plots of angle-of-attack stability measurements	19
Measured and calculated angle-of-attack stability measurements	20
Variation of speed-stability derivatives with tip-speed ratio	21

RESULTS AND DISCUSSION

Measured Rotor Characteristics

Measured rotor characteristics are presented in figures 5 to 11. Significant effects of high drag of the retreating blades, associated with blade stall, are shown in figures 6, 7, and 10. For example, the large rotor propulsive capability, equivalent to about 3 square feet of parasite-drag area, at a tip-path-plane angle of attack of 0.5°, is attributed to large drag forces on the retreating blades (fig. 10). The large rotor side forces, about the same as the rotor drag forces H, also indicate high blade drag at azimuth angles from 270° to 360° (fig. 7).

The variation of the equivalent rotor lift-drag ratio with thrust coefficient is given in figure 11. This ratio is a measure of rotor efficiency. Note that for the range of conditions investigated, the maximum thrusting efficiency

occurs at a thrust coefficient of about 0.005. The rapid decreases in rotor efficiency for $C_T > 0.005$ are the result of the previously noted increases in retreating blade drag.

Most of the lift-drag ratios shown are lower than those generally reported for full-scale lifting rotors, particularly at the negative attitude. (See, for example, ref. 3, pp. 240-243.) This result is in keeping with other indications in the tests of profile-power increases prior to conditions for stall.

Comparison of Measured and Calculated Rotor Performance

Comparisons of measured and calculated variations in thrust, power, and blade flapping motions with tip-speed ratio are shown in figures 12, 13, and 14 for measured thrust coefficients of 0.0035 and 0.0070. To further illustrate significant trends shown in these figures, the measured thrust, profile power, and longitudinal flapping are compared with refined-theory calculations in figures 15 and 16.

Thrust.- At the lower thrust coefficient (0.0035), no stall was anticipated, and the theoretical thrust values are in reasonable agreement with the measurements (figs. 13(a) and 14(a)). At the higher thrust coefficient (0.007), the commencement of stall is indicated, and, as expected, the simple theory predicts greater thrust than was measured. These differences are due to the neglect of reversed velocities as well as stall. Generally, at the higher tip-speed ratios where more blade stall was indicated, thrust calculated by the refined theory underpredicted measured values. These differences are interpreted as a delay in measured lift loss. At specific rotor tip-path-plane angles of attack and tip-speed ratios, these differences are large. (See fig. 15.) For example, at a measured mean-lift coefficient of 0.72, $\alpha_{TPP} = 0.5^{\circ}$, and $V/\Omega R = 0.246$, the measurements indicate about 30 percent more thrust than the refined theory predicts. Trends showing delays in lift loss, for conditions at which stall was theoretically predicted, were also noted in references 10 and 11.

Power.- The measured total power coefficient C_P and the rotor power coefficient $C_{P,i} + C_{P,o}$ are considerably greater than calculated values; this is particularly true near the predicted onset of stall. (See figs. 12, 13, and 14.) With the usual assumption that induced power can be predicted on a time-averaged, uniform-inflow basis, the earlier-than-predicted increase in measured power can be attributed to the profile power alone. Ratios of measured profile power to calculated profile power (based on refined theory, fig. 15) not only indicate that differences between measurements and calculations are large, but that these differences commence at relatively low lift coefficients. (See fig. 15.) An analysis of wind-tunnel tests of a 44-foot-diameter rotor indicates similar increases in measured profile power prior to the predicted onset of stall (ref. 11). Some differences would be expected, of course, because the present calculations do not consider the effects of surface roughness, Reynolds number, Mach number, or time rate of change of section angle of attack on the angle at which stall occurs. Also, it is suggested in reference 12 that consideration of the effects of nonuniform inflow and instantaneous induced velocities may be important in calculating induced power. This

earlier-than-expected rise in profile power has not always been noted in rotor performance tests. (See refs. 13 and 14, for example.)

In general, the calculated and measured parasite power are in poor agreement (figs. 12(b), 13(b), and 14(b)). The significance of these comparisons is that both the simple- and refined-theory calculations predict the rotor to be capable of producing a greater horizontal force than that measured for a given collective pitch and rotor attitude. The improved agreement of the refined theory with measurement for a thrust coefficient of 0.007 at tip-path-plane angles of attack of 10.5° and 0.5° results from predicted high section-drag coefficients on the retreating side of the rotor disk.

Flapping.- The differences between measured and calculated longitudinal flapping are in accordance with other stall trends discussed (figs. 12(c), 13(c), 14(c), and 16). The absolute values of measured and calculated longitudinal flapping show some correlation; however, there are noticeable differences in the rates at which the flapping increases with rotor lift. These differences are most pronounced at the nose-up rotor attitude (fig. 16(a)).

The lateral flapping characteristics are shown in figures 12(c), 13(c), and 14(c). Although the blades were stiff and the rotor had no built-in coning, the occurrence of lateral flapping can be accounted for by a small amount of blade bending and a longitudinal variation of inflow.

Correlation of Tuft Photographs With Performance Results

Tuft photographs showing the effects of increases in rotor lift on tuft flow patterns are presented in figure 17 for an average tip-speed ratio of 0.246. The photographs taken at zero mean-lift coefficient (figs. 17(b) and 17(c)) are intended to serve as a guide for evaluating the effects of blade lift on the tuft patterns.

Tuft position at zero lift is dependent not only upon the instantaneous direction of flow, but also upon the centrifugal forces acting on the tufts. Although spanwise boundary-layer flow due to centrifugal pumping may also have an effect on tuft position, the effect is believed to be small at zero lift. (See ref. 15.)

In general, it is impossible to separate the various flow effects on the tufts at high lift coefficients; however, where the ends of the tufts point toward the leading edge or where they are lifted from the blade surface (casting a shadow), the predominant effect is believed to be local flow separation. In some instances, the tufts may have lifted from the blade surface but did not cast a shadow because of the flash-lamp orientation. Tuft photographs taken during repeat tests are generally in good agreement with those presented herein. However, some differences in tuft position, particularly for the radially oriented tufts, were noted at the higher mean-lift coefficients; this suggests that the flow was unsteady and possibly separated.

Lift.- Calculated contours of section angles of attack are presented in figure 18. In the azimuth region from 180° to 240° the contours indicate

local section angles of attack as high as 20° at $\overline{C}_L = 0.816$ (fig. 18(b)); however, a comparison of the tuft photograph at this lift coefficient with that at $\overline{C}_L = 0.530$ (fig. 18(a)) shows that no appreciable flow change was present. The spacing of the contours in figure 18(b) suggests very high rates of increase of section angles of attack in this region. Such time-rate increases in angle of attack for wings have been shown to result in delays in flow separation to angles greater than the steady-state stall angle, with accompanying instantaneous lift greater than the maximum steady-state value. (See refs. 16 to 18.) More recently, these trends have been shown to exist for rotors (ref. 19). Experimental results important in understanding this effect on rotors are presented in reference 20. The results indicate that airfoils oscillating at mean angles of attack equal to or less than the steady-state stall angles produce a time-averaged lift approximately equal to the steady-state lift at the mean angle of attack, even though the instantaneous angles greatly exceeded the steady-state stall angle. The changes of blade-section angles of attack during one rotor revolution are somewhat analogous to these airfoil oscillations. However, it is not known if the inclusion of unsteady airfoil section characteristics in rotor calculations would completely explain the delay in flow changes indicated by the tufts or the delays in lift loss shown in figure 15.

Profile power.- The calculated contours of section angles of attack shown in figure 18(a) indicate that the rotor is operating with only a slight amount of blade-tip stall ($\overline{C}_L = 0.530$, $\alpha_{TPP} = 0.5^{\circ}$, $V/\Omega R = 0.246$). However, tuft patterns and the ratios of measured profile power to calculated profile power (fig. 15(b)) indicate that a large amount of local flow separation and/or an equivalent drag-producing flow was present for this condition. In order to explore possible explanations for these differences, an approximate analysis using time-averaged nonuniform inflow theory was made (ref. 1). This analysis accounted for only a portion of the differences between measured and calculated profile power. However, it did show additional areas in which stall should be expected.

At present it is not known if power increases due to centrifugal pumping or time-rate changes in section angle of attack would significantly affect power requirements. Other factors contributing to differences between measured and calculated profile power have been discussed previously.

Static Stability With Angle of Attack

Measurements for large changes in rotor-shaft angle of attack were made at initial trim rotor tip-path-plane angles of attack of -9.5° and 0.5°; that is, the rotor was initially trimmed normal to the shaft, and the shaft angle of attack was then increased in 5° increments with the rotor controls fixed.

Incremental changes in the measured data from the trim values are presented in figure 19 for average tip-speed ratios from 0.246 to 0.538. As with the performance measurements, the thrust increments did not show the thrust losses expected when stall was believed present. (Note the linearity of the ΔC_T curves in fig. 19.) Also, unexpected decreases in the angle of the resultant-force vector a' were noted for increases in shaft angle. These trends

indicate rotor stability with a change in angle of attack for a fuselage center of gravity located below the rotor plane.

Data for two representative thrust conditions are compared with calculations in figures 20 and 21. Figure 20(a) presents data taken for an initial trimmed C_T of 0.0045, which is below the theoretical onset of rotor blade-section stall. Increases in shaft angle of attack, as discussed previously, did not result in the decrease in the rate of change of thrust predicted by refined theory. On the other hand, the power coefficients indicate a power rise above that predicted by the simple unstalled theory. This power rise occurs primarily on the retreating side of the rotor disk, as is evidenced by a reversal of the in-plane drag coefficient C_H. Reversals of rotor in-plane force and, consequently, the angle of the resultant-force vector have also been noted in other rotor tests. (See, for example, refs. 21 and 22.)

The rotor longitudinal flapping coefficients a_1 give further indication that this rotor did not stall in the manner predicted by the refined theory: for example, at $\frac{V}{\Omega R} = 0.25$ the changes in longitudinal flapping are predicted almost exactly by the simple unstalled theory.

The combination of increasing thrust, decreasing in-plane force, and small positive changes in longitudinal flapping is by definition a trend toward angle-of-attack stability. This trend is exhibited by the decrease in a' with increasing shaft angle of attack. Note that the refined-theory calculations show a perceptible dip in the curve of $\Delta a'$ for the range of shaft angles at which the rotor was not severely stalled. In order to establish the sensitivity of the a' calculation to the two-dimensional section characteristics, several calculations were made with different section data for blade-section angles greater than 12°. These calculations are not presented herein, but the following results were noted: For a small increase in section-drag coefficient, the dip in the calculated $\Delta a'$ curve was increased and the values became negative. By assuming a constant lift-curve slope and by using the increased section-drag coefficients, calculated values of $\Delta a'$ produced essentially the same trends as the measured data.

Figure 20(b) presents data for an initial trim thrust coefficient C_T of 0.0090 which, according to theory, should be a stalled condition. A comparison of the rates of change of thrust with shaft angle of attack for the two test conditions $\left(C_T = 0.0045 \text{ and } C_T = 0.0090\right)$ shown in figures 20(a) and 20(b) indicates no appreciable decrease in slope for the higher thrust condition where blade-section stall is expected to be more severe. The larger negative increment of the resultant-force-vector angle at the higher thrust condition, however, does indicate a greater increase in the drag force on the retreating side of the disk than was noted at the lower thrust.

It should not be taken for granted that these stabilizing trends will occur on flight vehicles; for example, adverse periodic twist (contributing instability) is to be expected on more flexible blades. However, there are indications in the tests of the 44-foot-diameter rotor of reference 11 that these trends did exist, although to a lesser degree than noted herein.

Static Stability With Speed

Measured and calculated static stability, with respect to velocity changes, is presented in figure 21 for trim thrust coefficients of approximately 0.0045. A rearward tilt of the resultant-force vector for an increase in forward speed is defined as a stable variation $\left(\text{i.e., a rearward tilt opposes the increase in speed, } \frac{\partial a'}{\partial(V/\Omega R)} > 0\right)$. As expected, both measurements and calculations indicate that the rotor is statically stable with speed for the conditions investigated. In some early stability analyses it was found convenient to ignore the rotor in-plane drag coefficient C_H and assume that changes in longitudinal flapping represented changes in the resultant-force-vector tilt a'. Note the good agreement between measured a_1 and a' derivatives at low tip-speed ratios. However, the present results and theoretical studies (ref. 23) indicate that this assumption can result in large errors. The differences between a_1 and a' derivatives at higher tip-speed ratios always reflect the effects of in-plane rotor drag. For example, the trend toward instability with speed of the a' derivative at a constant value of α_{TPP} of 10.5° is primarily due to a trend for the rotor drag to decrease because of the high drag of the retreating blades. As with the performance comparisons, the calculated derivatives did not show consistent correlations with the derivatives obtained from measured data when stall was expected.

SUMMARY OF RESULTS

Results of wind-tunnel tests of a lifting rotor operating at conditions expected to produce large amounts of blade stall indicate that:

1. At conditions free of calculated blade stall, the measured and calculated thrusts were in good agreement. However, when stall was theoretically predicted, the measured thrust indicated a delay in lift loss.

2. For conditions near the onset of stall, measured rotor profile power was significantly greater than predicted by theory.

3. Calculated rotor propulsive forces, for a given collective pitch and rotor attitude, were greater than measured.

4. The longitudinal rotor flapping did not show any sudden divergence when stall was encountered.

5. Stall induced by large changes in shaft angle of attack caused the rotor to exhibit stabilizing trends for large changes in shaft angle of attack.

The extent to which these interesting (and in many cases unexpected) trends at extreme thrust and stall conditions are peculiar to the test airfoil section and Reynolds number is not known. However, the airfoil section is in common use, and the Reynolds number is the same as that for some small-size helicopters.

In view of these facts, these tests indicate that very small helicopters, at least, may not react as expected when blade stall is present. Also, an examination of other test results indicates that some of these trends can be expected to appear in varying degrees with larger rotors.

Langley Research Center,
National Aeronautics and Space Administration,
Langley Station, Hampton, Va., June 17, 1964.

REFERENCES

1. Sweet, George E., and Jenkins, Julian L., Jr.: Results of Wind-Tunnel Measurements on a Helicopter Rotor Operating at Extreme Thrust Coefficients and High-Tip-Speed Ratios. Jour. American Helicopter Soc., vol. 8, no. 3, July 1963, pp. 4-9.

2. Heyson, Harry H.: Linearized Theory of Wind-Tunnel Jet-Boundary Corrections and Ground Effect for VTOL-STOL Aircraft. NASA TR R-124, 1962.

3. Gessow, Alfred, and Myers, Garry C., Jr.: Aerodynamics of the Helicopter. The Macmillan Co., c.1952.

4. Sweet, George E.: Hovering Measurements for Twin-Rotor Configurations With and Without Overlap. NASA TN D-534, 1960.

5. Payne, P. R.: Helicopter Dynamics and Aerodynamics. The Macmillan Co., 1959, p. 197.

6. Bailey, F. J., Jr.: A Simplified Theoretical Method of Determining the Characteristics of a Lifting Rotor in Forward Flight. NACA Rep. 716, 1941.

7. Gessow, Alfred: Equations and Procedures for Numerically Calculating the Aerodynamic Characteristics of Lifting Rotors. NACA TN 3747, 1956.

8. Gessow, Alfred, and Crim, Almer D.: A Method for Studying the Transient Blade-Flapping Behavior of Lifting Rotors at Extreme Operating Conditions. NACA TN 3366, 1955.

9. Critzos, Chris C., Heyson, Harry H., and Boswinkle, Robert W., Jr.: Aerodynamic Characteristics of NACA 0012 Airfoil Section at Angles of Attack From 0° to 180°. NACA TN 3361, 1955.

10. Clarke, A. E.: Recent Work at the Royal Aircraft Establishment on Helicopter Dynamic Loads, With Particular Reference to High Blade Incidence Problems. Paper presented at CAL/TRECOM symposium on Dynamic Load Problems Associated With Helicopters and V/STOL Aircraft (Buffalo, N.Y.), June 26-28, 1963.

11. McCloud, John L., III, and McCullough, George B.: Comparison of Calculated and Measured Stall Boundaries of a Helicopter Rotor at Advance Ratios From 0.3 to 0.4. NASA TN D-73, 1959.

12. Piziali, Raymond, and DuWaldt, Frank: Computed Induced Velocity, Induced Drag, and Angle of Attack Distributions for a Two-Bladed Rotor. Paper presented at Nineteenth Annual National Forum, American Helicopter Soc., Inc. (Washington, D.C.), May 1-3, 1963.

13. Gustafson, F. B., and Gessow, Alfred: Effect of Blade Stalling on the Efficiency of a Helicopter Rotor As Measured in Flight. NACA TN 1250, 1947.

14. McCloud, John L., III, Biggers, James C., and Maki, Ralph L.: Full-Scale Wind-Tunnel Tests of a Medium-Weight Utility Helicopter at Forward Speeds. NASA TN D-1887, 1963.

15. Graham, Martha E.: Calculation of Laminar Boundary Layer Flow on Rotating Blades. Contract No. AF 33(038)-21406, Graduate School Aero. Eng., Cornell Univ., Sept. 1954.

16. Hinton, S. H., and Lodge, D. W.: Application of Boundary Layer Control to Helicopter Rotor Blades. Rep. No. 1360 (Contract No. NONR-898(00)), Cessna Aircraft Co., Feb. 29, 1956.

17. Harper, Paul W., and Flanigan, Roy E.: The Effect of Rate of Change of Angle of Attack on the Maximum Lift of a Small Model. NACA TN 2061, 1950.

18. Harper, Paul W., and Flanigan, Roy E.: Investigation of the Variation of Maximum Lift for a Pitching Airplane Model and Comparison With Flight Results. NACA TN 1734, 1948.

19. Scheiman, James, and Kelley, Henry L.: Comparison of Flight Measured Helicopter Rotor Blade Chordwise Pressure Distributions and Two-Dimensional Airfoil Characteristics. CAL/TRECOM Symposium Proceedings Vol I - Dynamic Load Problems Associated With Helicopters and V/STOL Aircraft, June 1963.

20. Halfman, Robert L., Johnson, H. C., and Haley, S. M.: Evaluation of High-Angle-of-Attack Aerodynamic-Derivative Data and Stall-Flutter Prediction Techniques. NACA TN 2533, 1951.

21. Owen, T. B., Fail, R., and Eyre, R. C. W.: Wind Tunnel Tests on a Six-Foot Diameter Helicopter Rotor. Tech. Note No. Aero 2378, British R.A.E., May 1955.

22. Squire, H. B., Fail, R. A., and Eyre, R. C. W.: Wind-Tunnel Tests on a 12-Foot Diameter Helicopter Rotor. R. & M. No. 2695, British A.R.C., 1953.

23. Amer, Kenneth B., and Gustafson, F. B.: Charts for Estimation of Longitudinal-Stability Derivatives for a Helicopter Rotor in Forward Flight. NACA TN 2309, 1951.

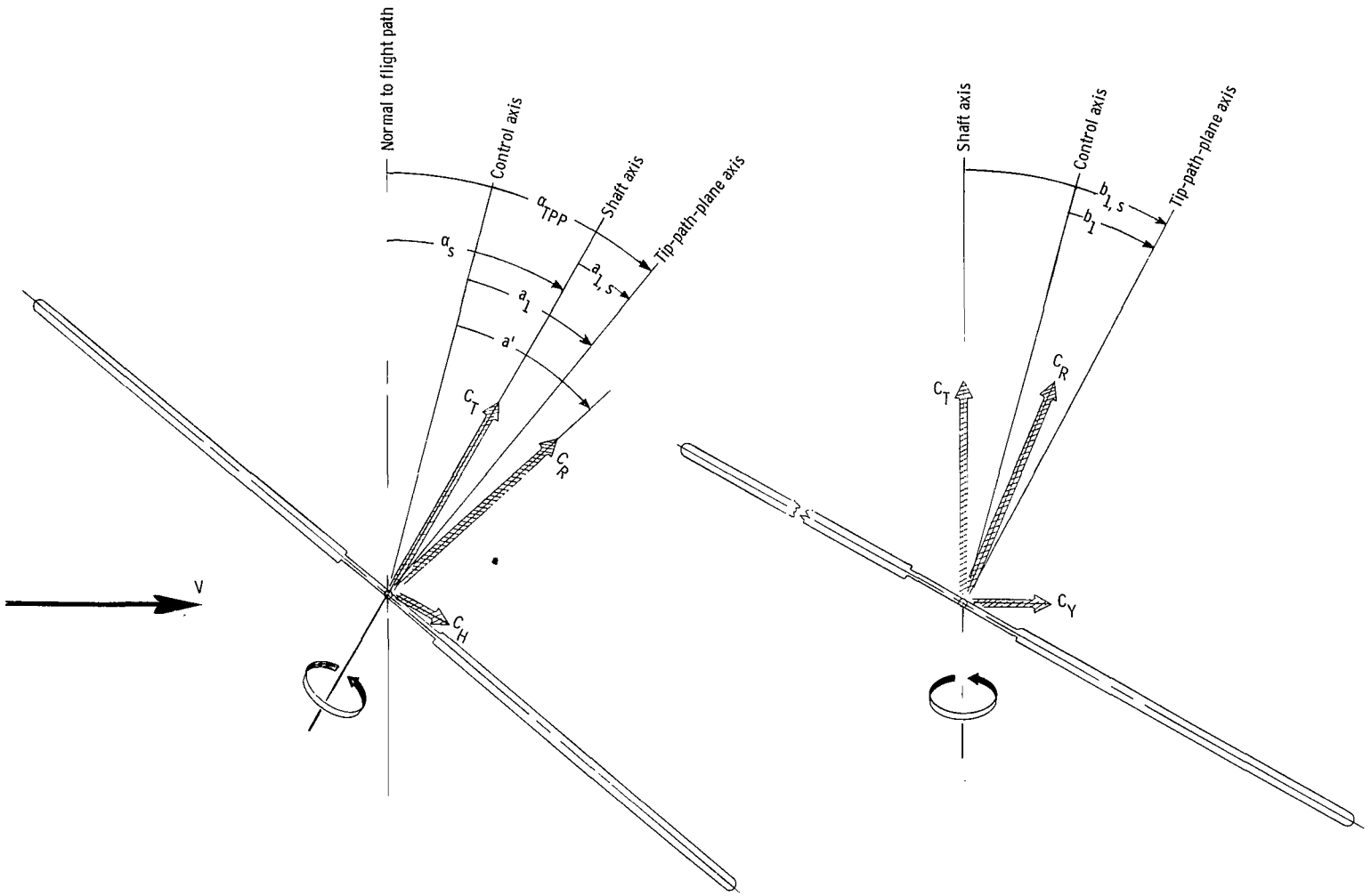

(a) Side view.

(b) Rear view.

Figure 1.- Notation showing the positive directions of forces and angles.

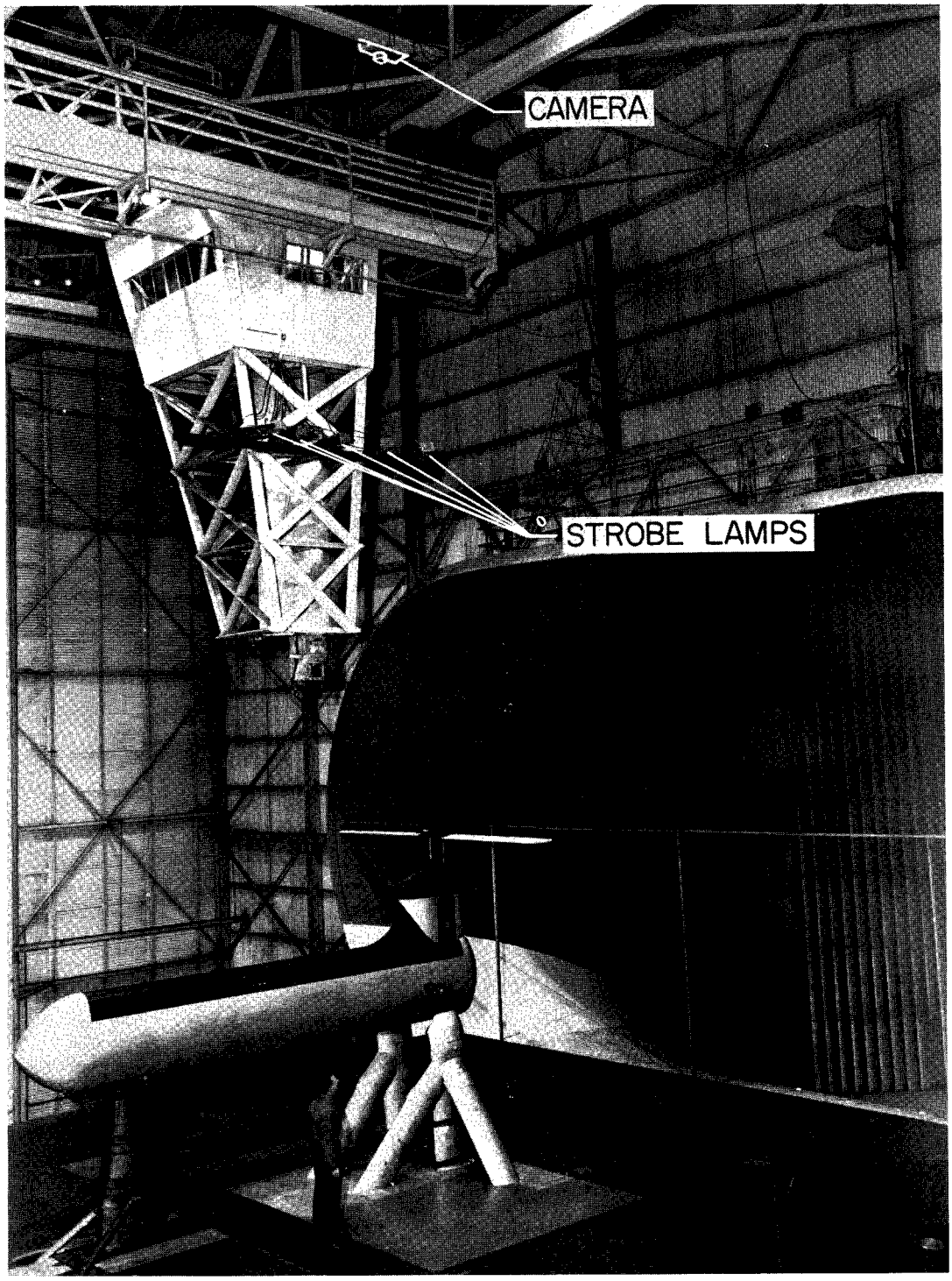

Figure 2.- General view of the test equipment. L-62-3093.1

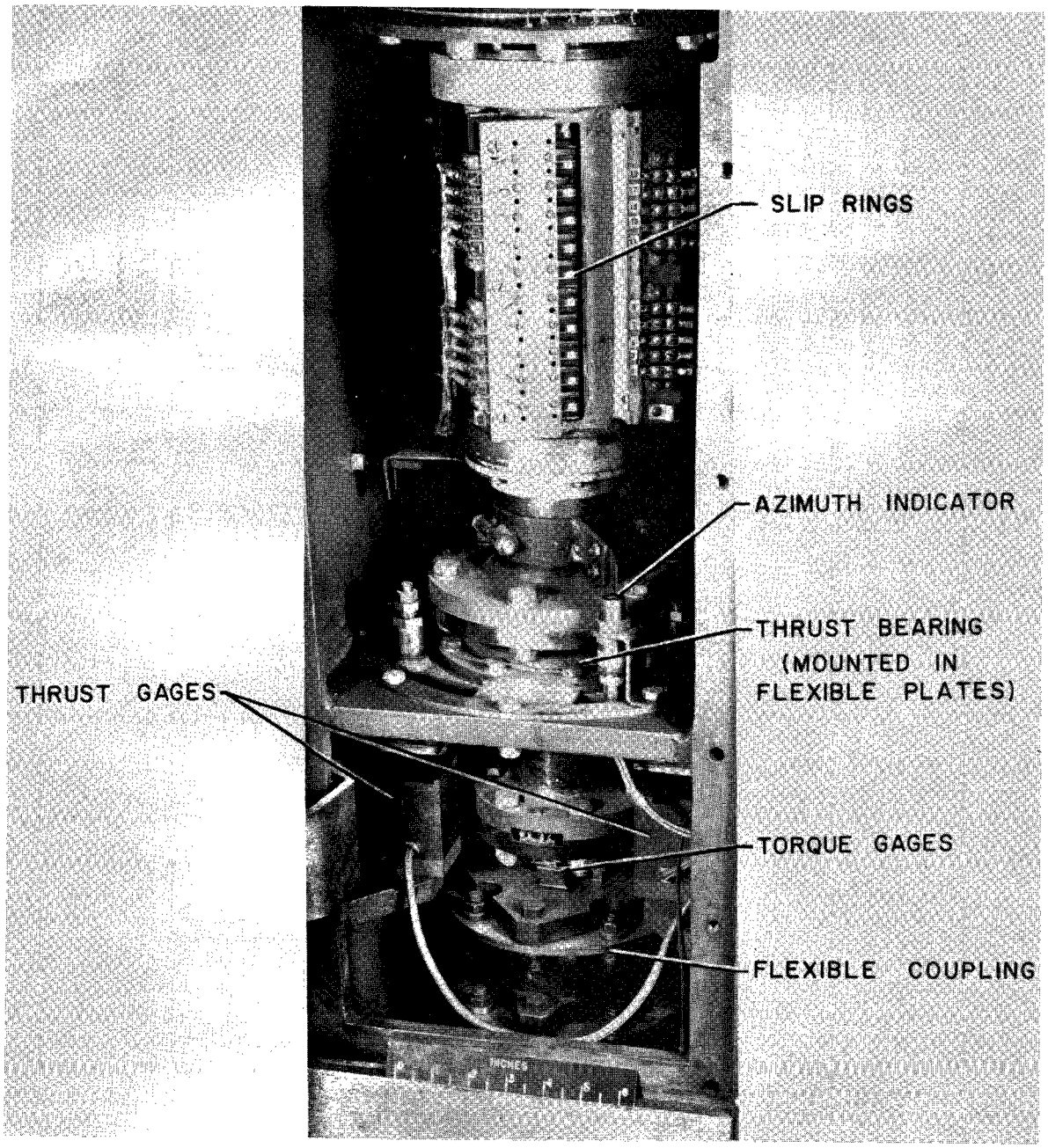

Figure 3.- Force measuring system. L-58-621a.1

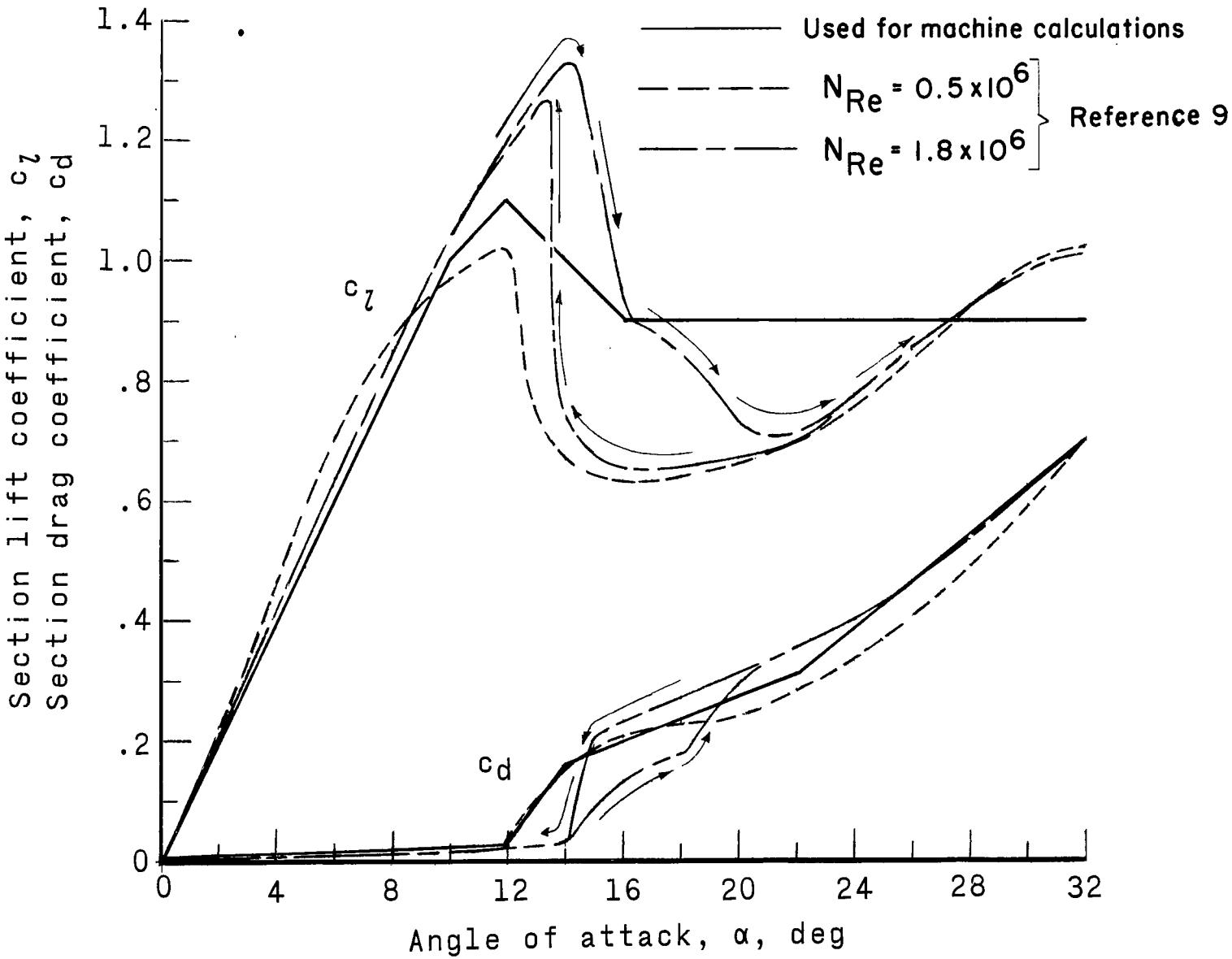

Figure 4.- Comparison of measured section characteristics of the 0012 airfoil with those used in machine calculations. Measured characteristics are for a smooth airfoil surface.

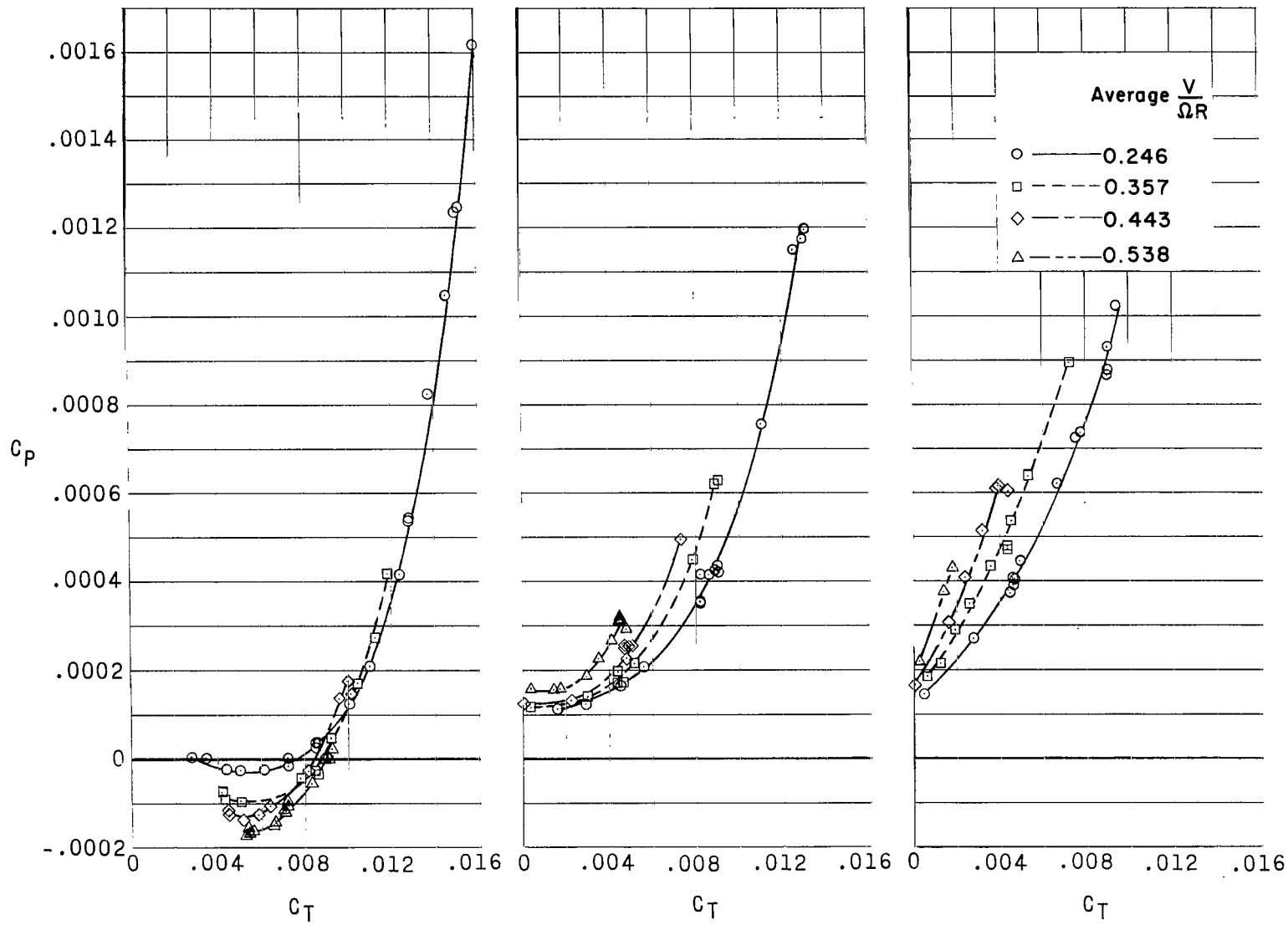

(a) $\alpha_{TPP} = 10.5^{\circ}$.

(b) $\alpha_{TPP} = 0.5^{\circ}$.

(c) $\alpha_{TPP} = -9.5^{\circ}$.

Figure 5.- Variation of total-rotor-power coefficient with thrust coefficient and tip-speed ratio.

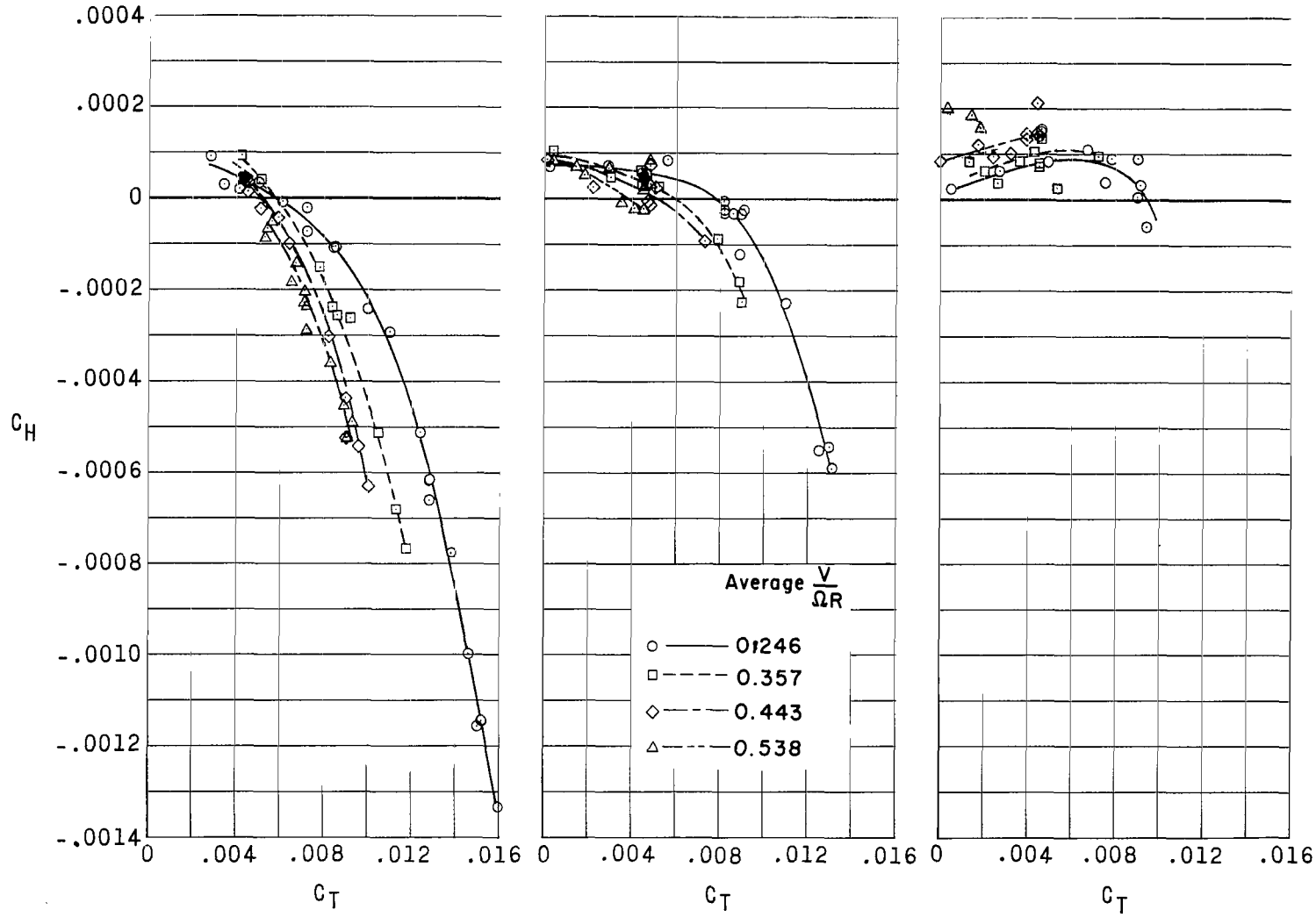

(a) $\alpha_{TPP} = 10.5^{\circ}$.

(b) $\alpha_{TPP} = 0.5^{\circ}$.

(c) $\alpha_{TPP} = -9.5^{\circ}$.

Figure 6.- Variation of rotor H-force coefficient with thrust coefficient and tip-speed ratio.

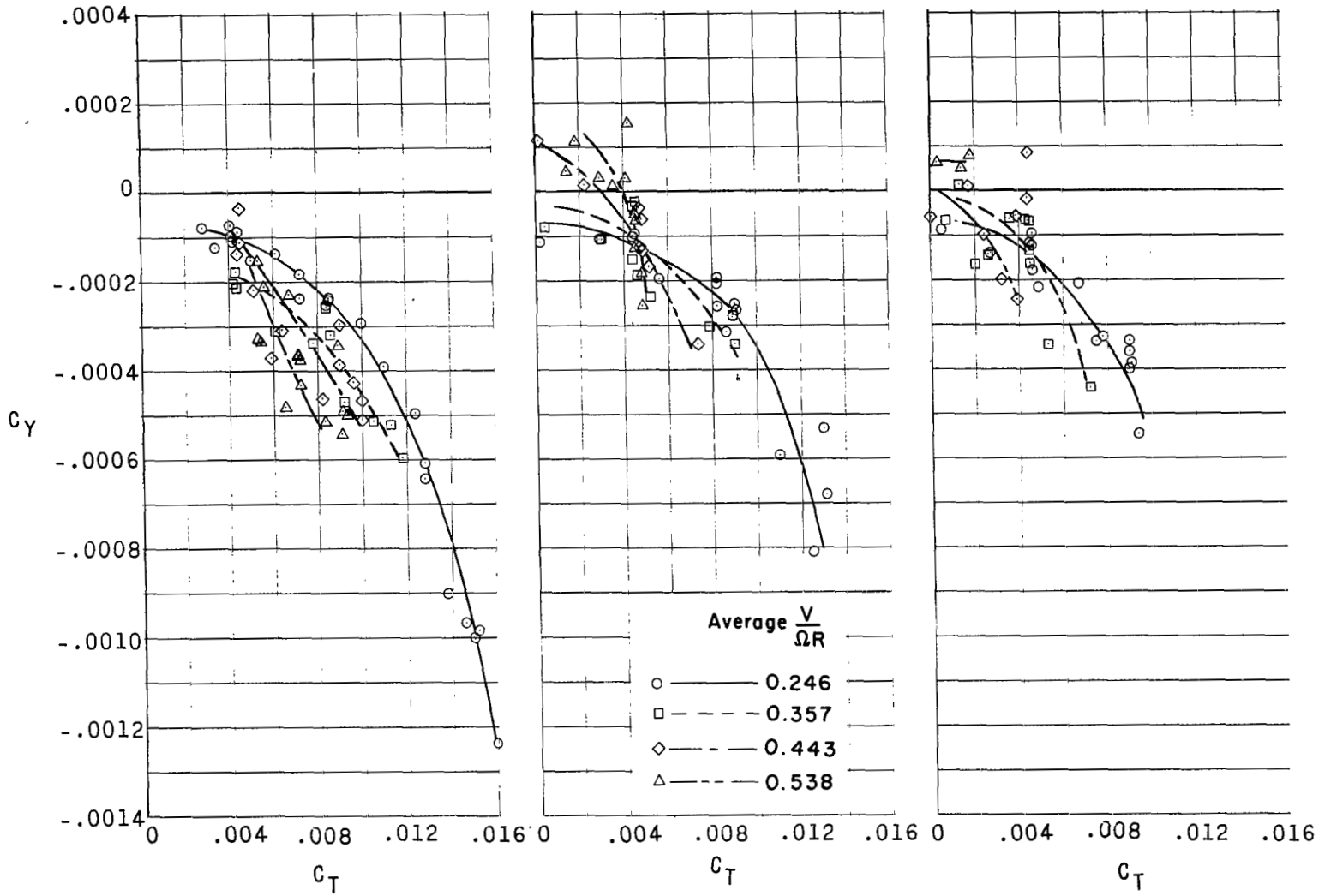

(a) $\alpha_{TPP} = 10.5^{\circ}$.

(b) $\alpha_{TPP} = 0.5^{\circ}$.

(c) $\alpha_{TPP} = -9.5^{\circ}$.

Figure 7.- Variation of rotor side-force coefficient with thrust coefficient and tip-speed ratio.

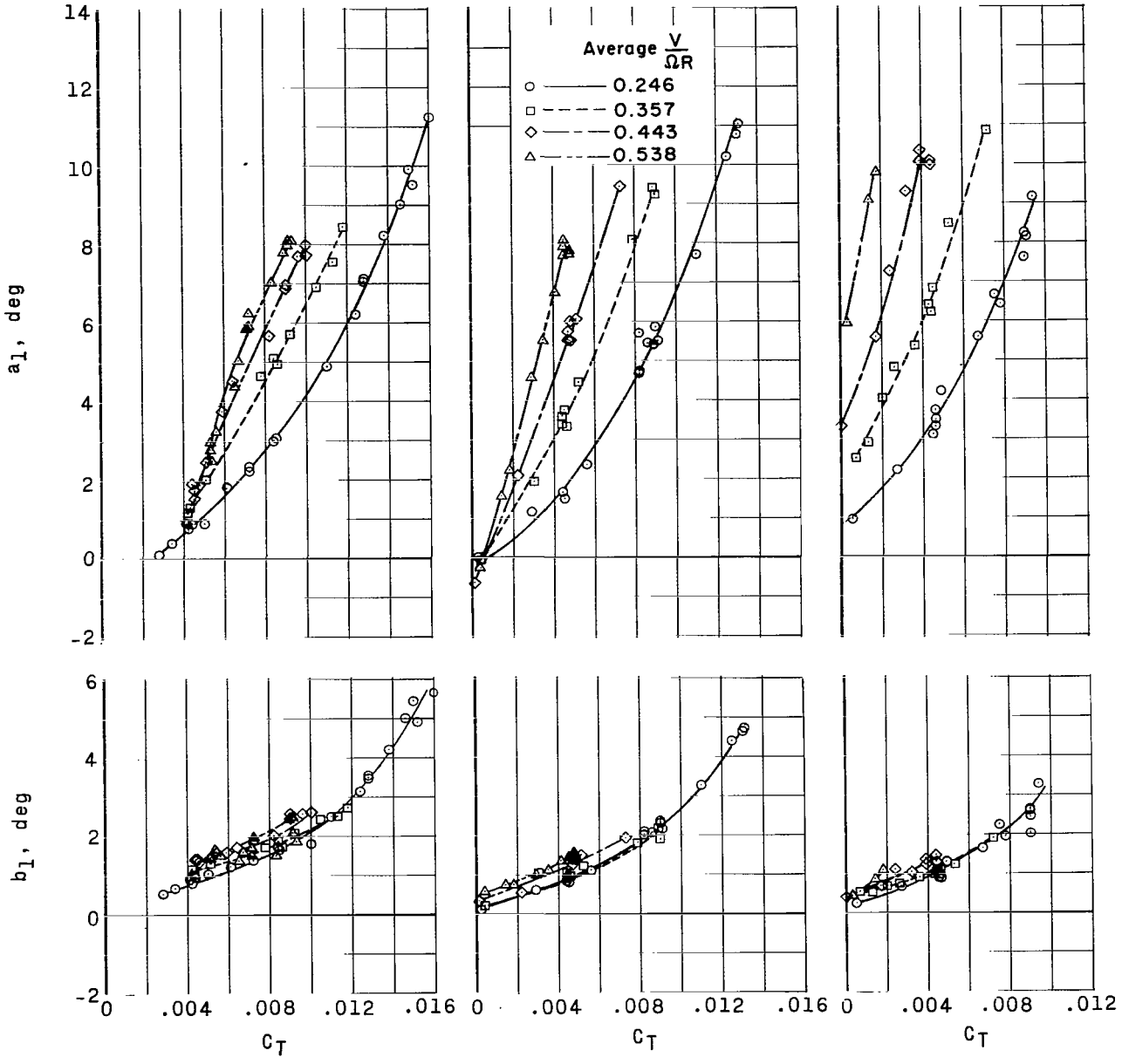

(a) $\alpha_{TPP} = 10.5^{\circ}$. (b) $\alpha_{TPP} = 0.5^{\circ}$. (c) $\alpha_{TPP} = -9.5^{\circ}$.

Figure 8.- Variation of equivalent longitudinal and lateral flapping coefficients with thrust coefficient and tip-speed ratio.

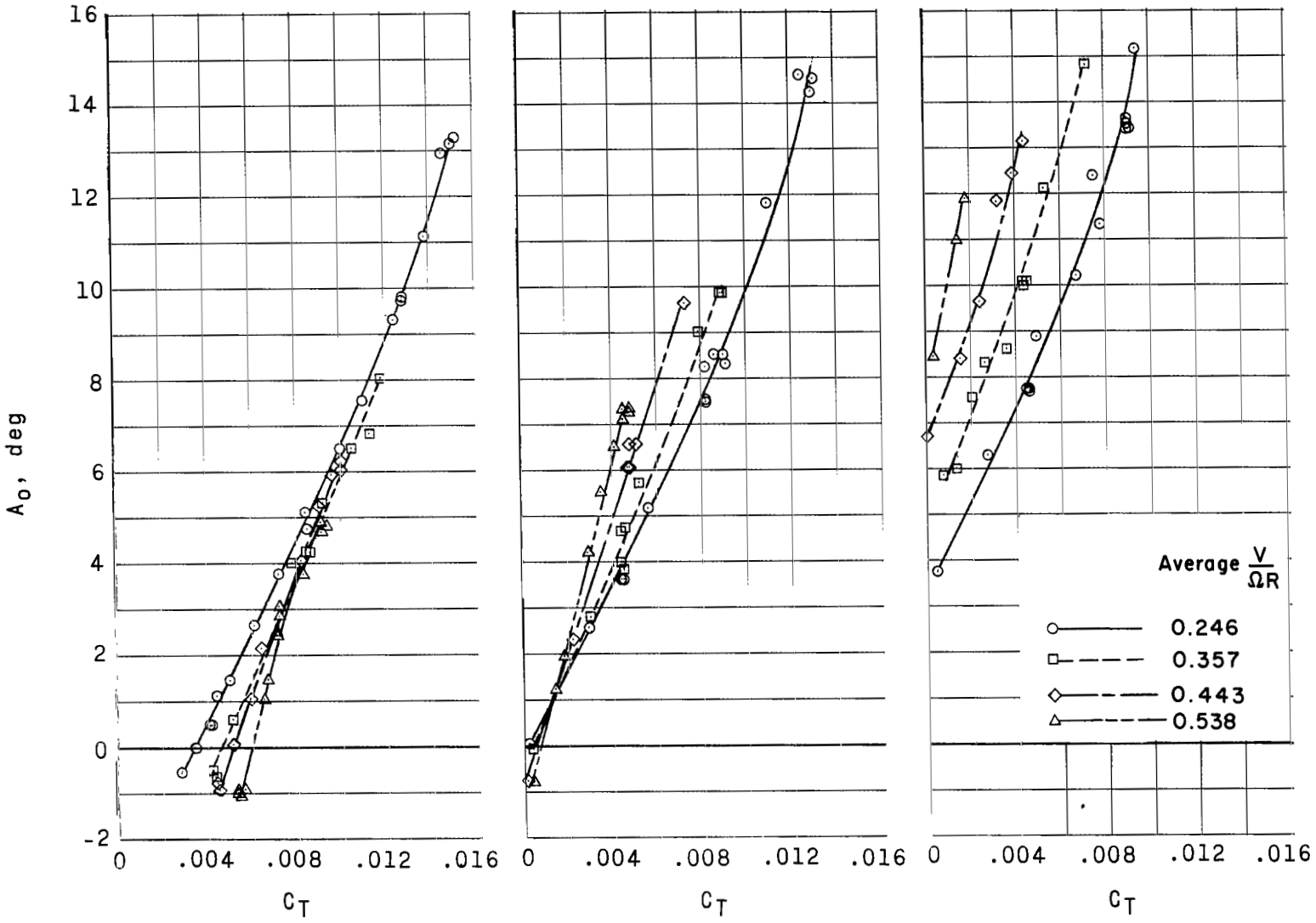

(a) α_{TPP} = 10.5°.

(b) α_{TPP} = 0.5°.

(c) α_{TPP} = -9.5°.

Figure 9.- Variation of collective pitch with thrust coefficient and tip-speed ratio.

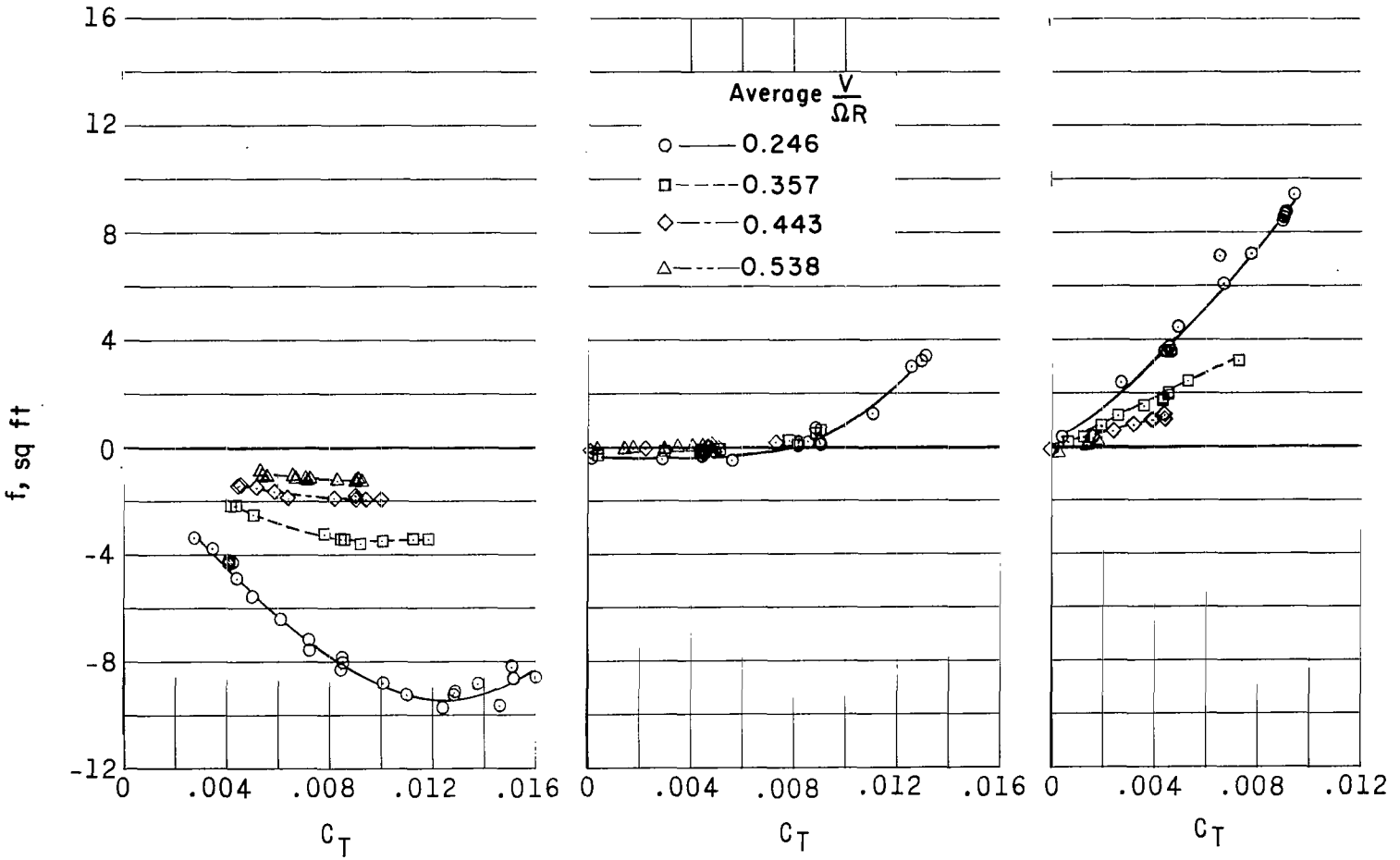

(a) $\alpha_{TPP} = 10.5^{\circ}$.

(b) $\alpha_{TPP} = 0.5^{\circ}$.

(c) $\alpha_{TPP} = -9.5^{\circ}$.

Figure 10.- Rotor propulsive capability in terms of equivalent parasite-drag area.

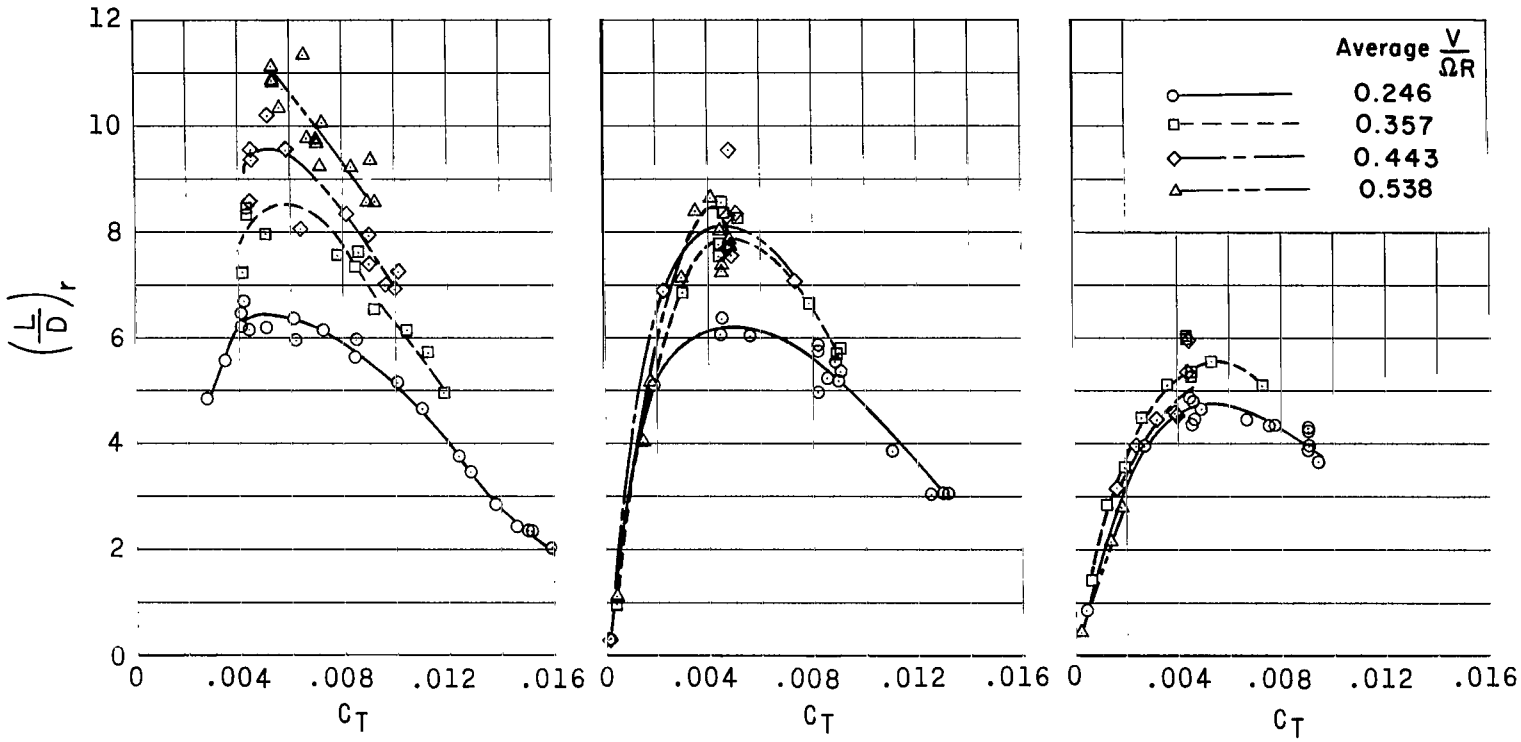

(a) $\alpha_{TPP} = 10.5^{\circ}$.

(b) $\alpha_{TPP} = 0.5^{\circ}$.

(c) $\alpha_{TPP} = -9.5^{\circ}$.

Figure 11.- Variation of equivalent rotor lift-drag ratio with thrust coefficient and tip-speed ratio.

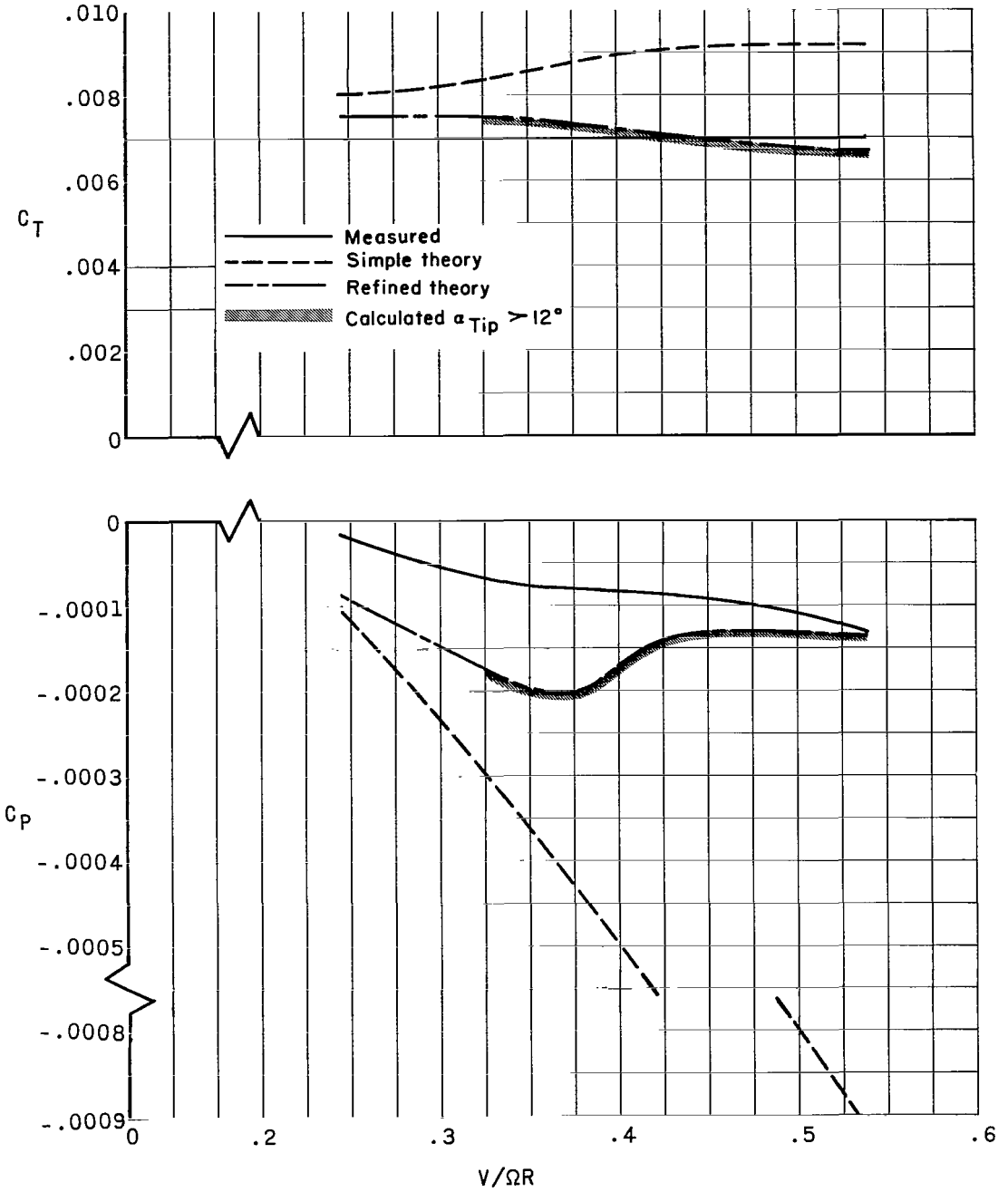

(a) Thrust and total-power coefficients.

Figure 12.- Comparison of measured and calculated rotor performance and flapping motions. Calculations are based on measured collective pitch and feathering motions. $\alpha_{TPP} = 10.5^{\circ}$; $C_T = 0.007$.

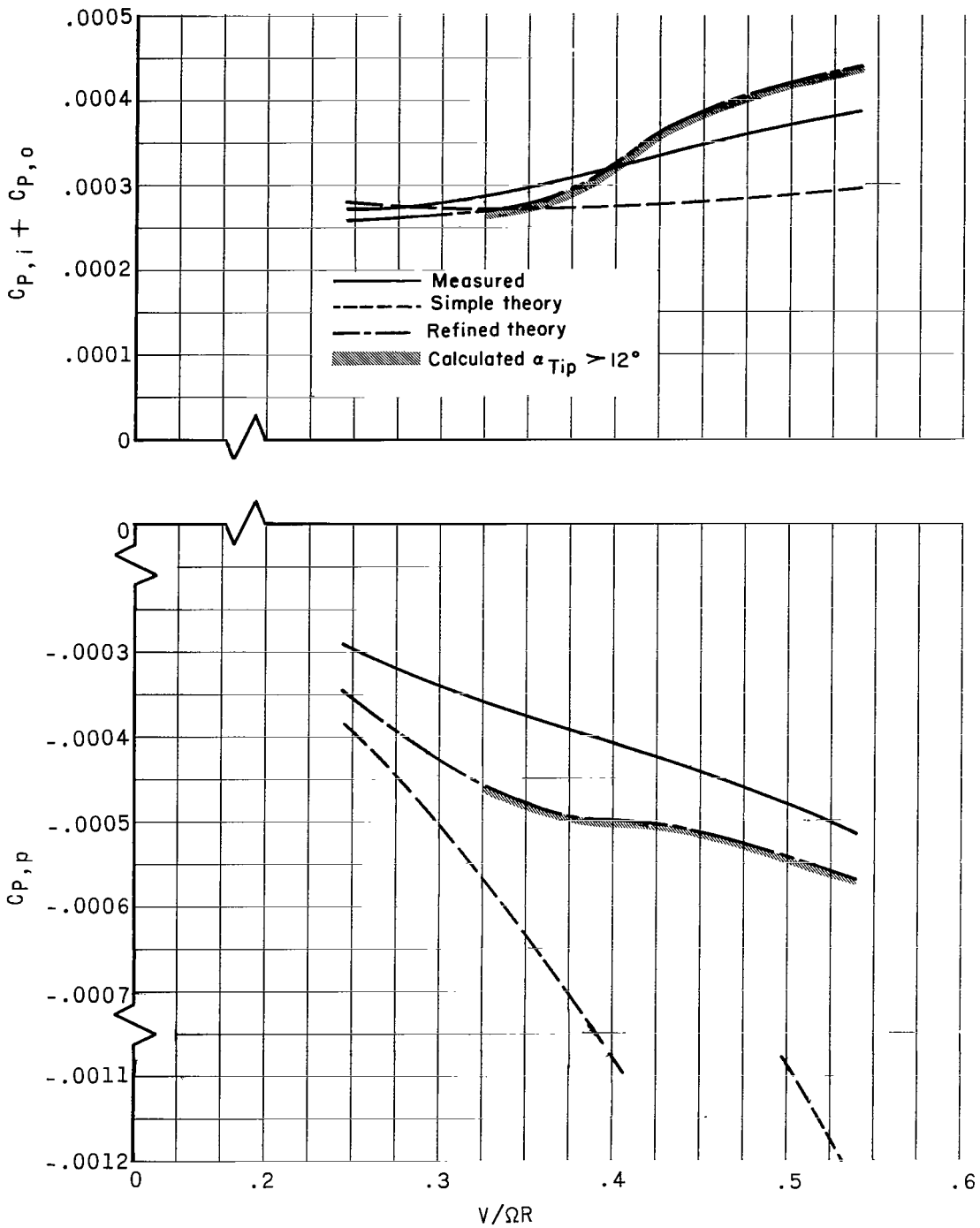

(b) Rotor-power and parasite-power coefficients.

Figure 12.- Continued.

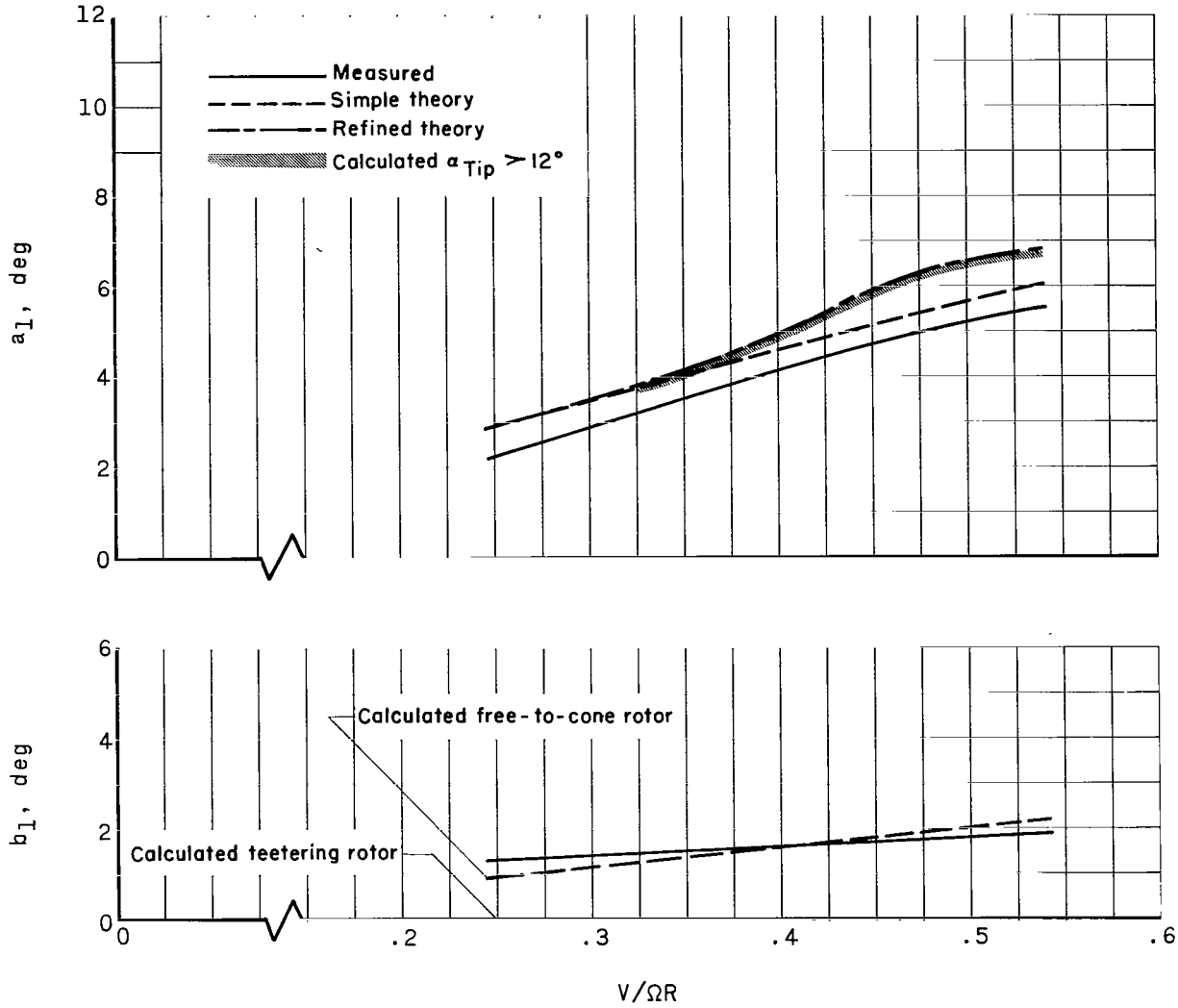

(c) Equivalent longitudinal and lateral flapping coefficients.

Figure 12.- Concluded.

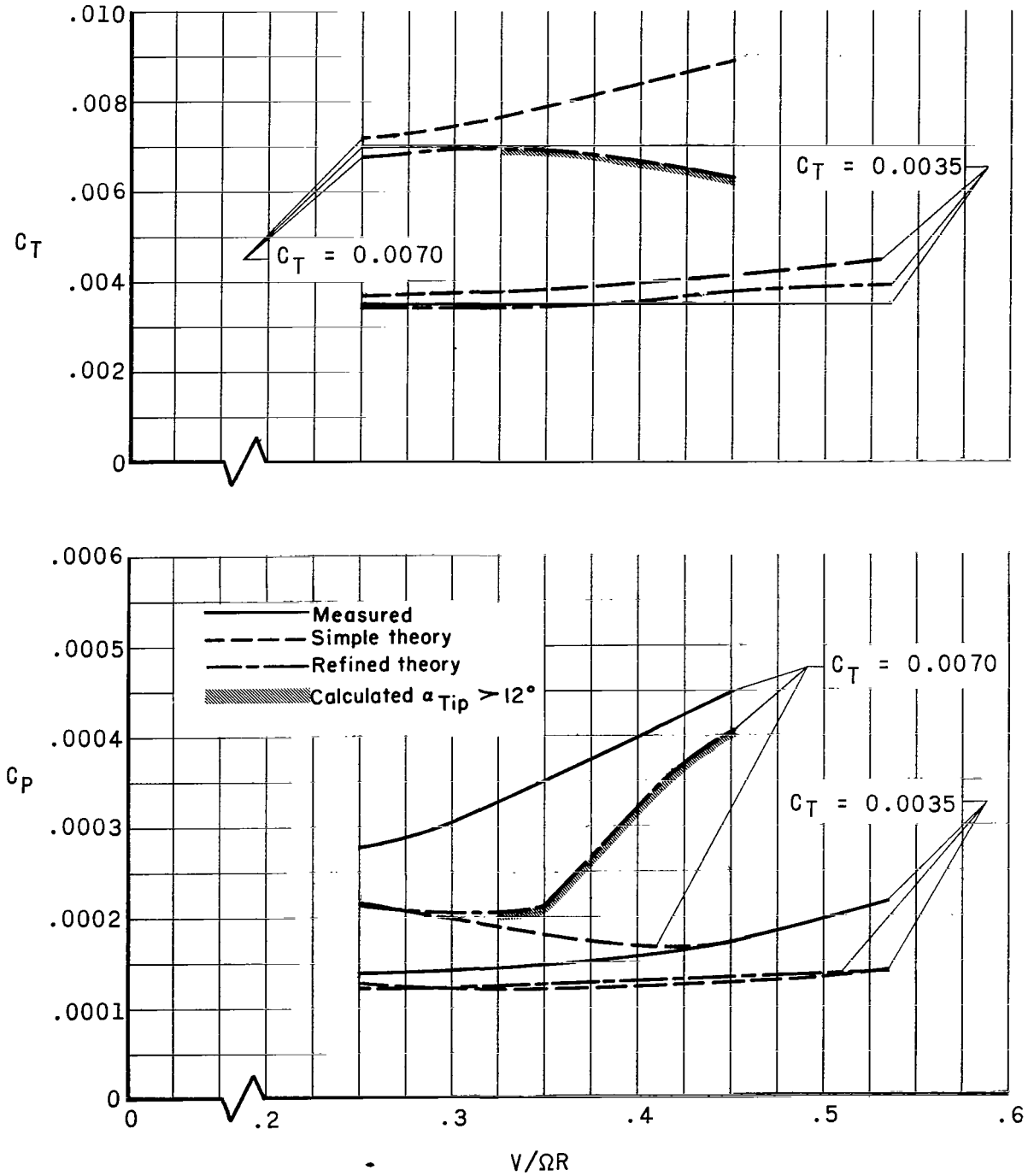

(a) Thrust and total-power coefficients.

Figure 13.- Comparison of measured and calculated rotor performance and flapping motions. Calculations are based on measured collective pitch and feathering motions. $\alpha_{TPP} = 0.5°$.

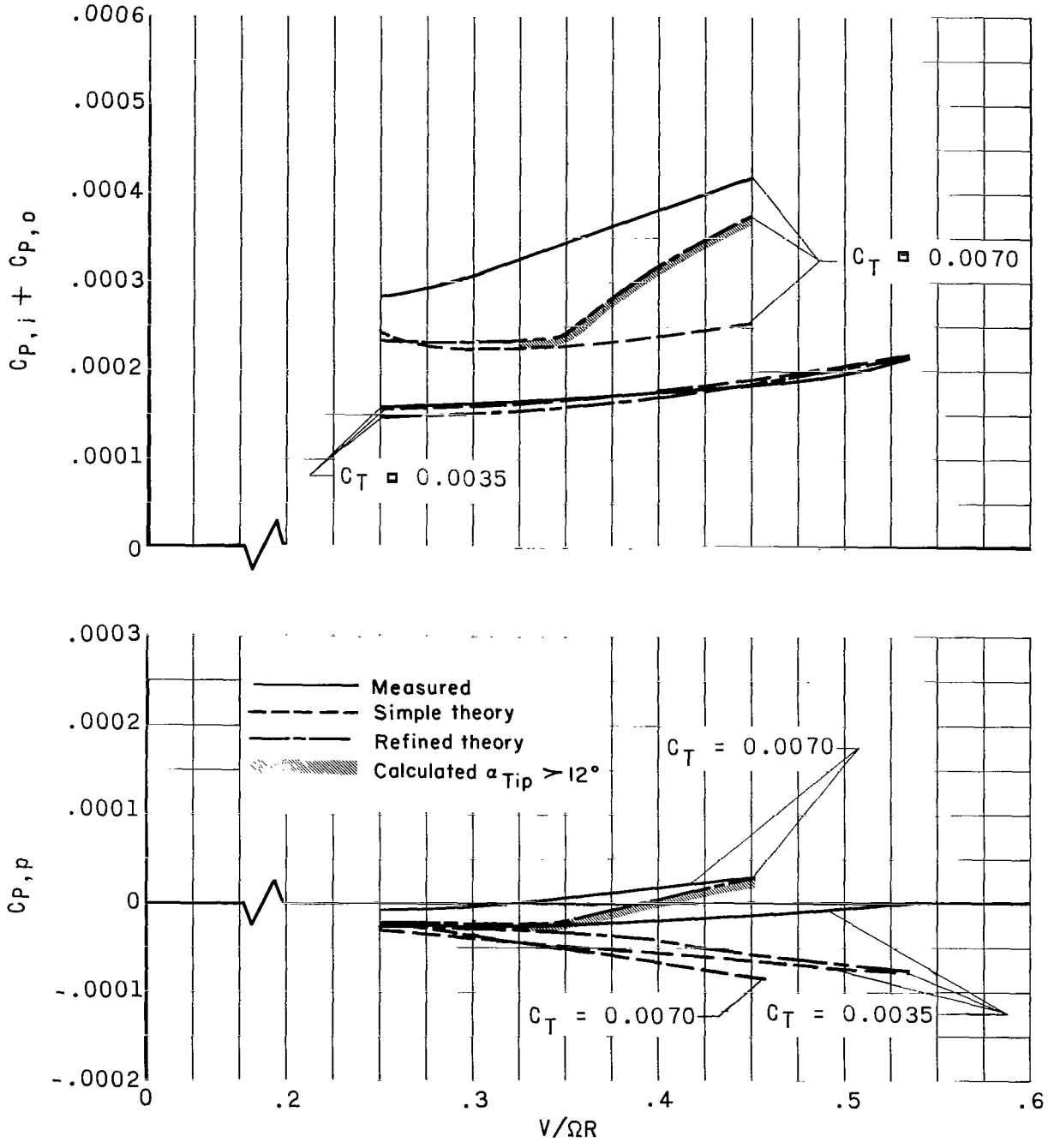

(b) Rotor-power and parasite-power coefficients.

Figure 13.- Continued.

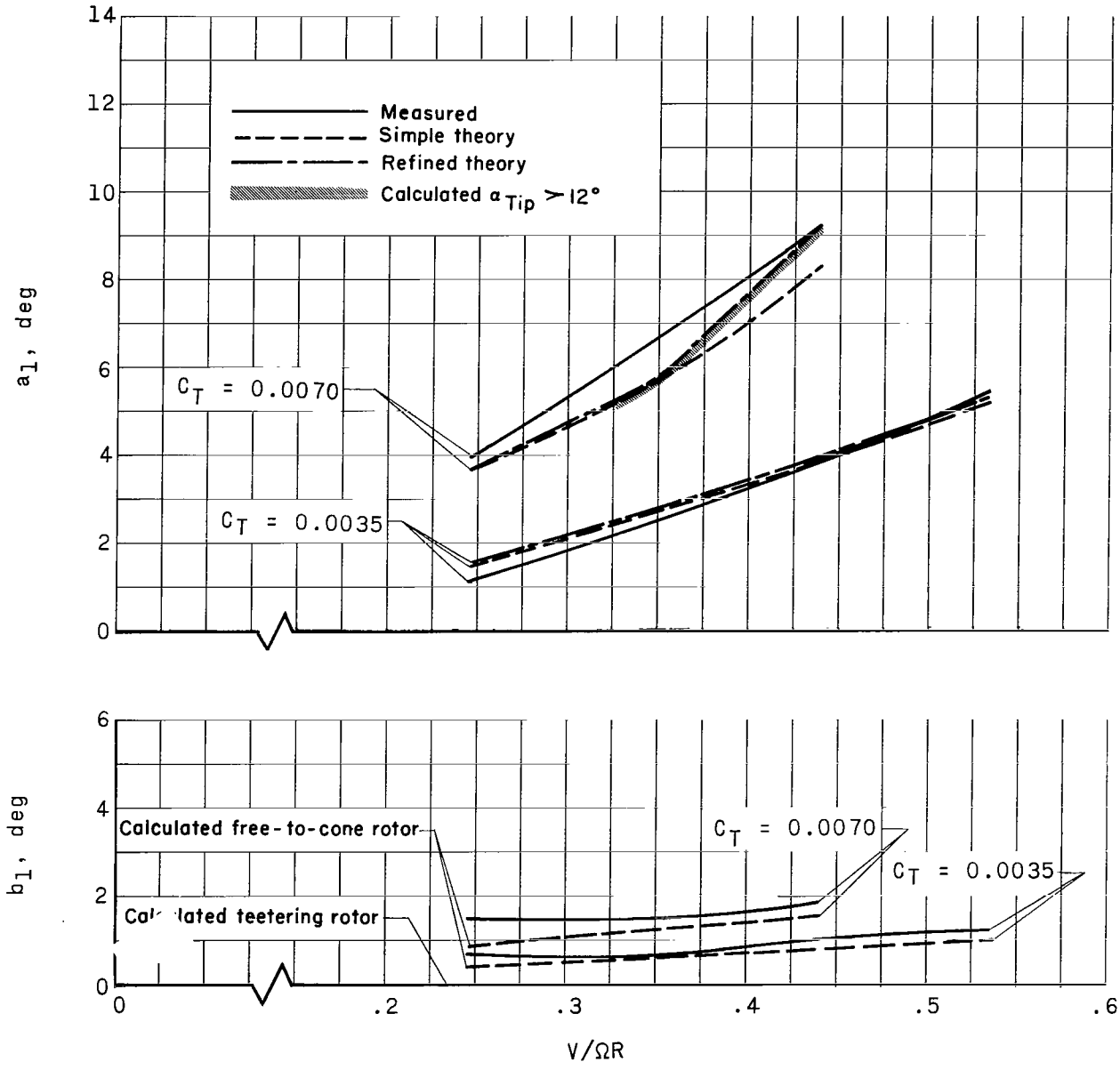

(c) Equivalent longitudinal and lateral flapping coefficients.

Figure 13.- Concluded.

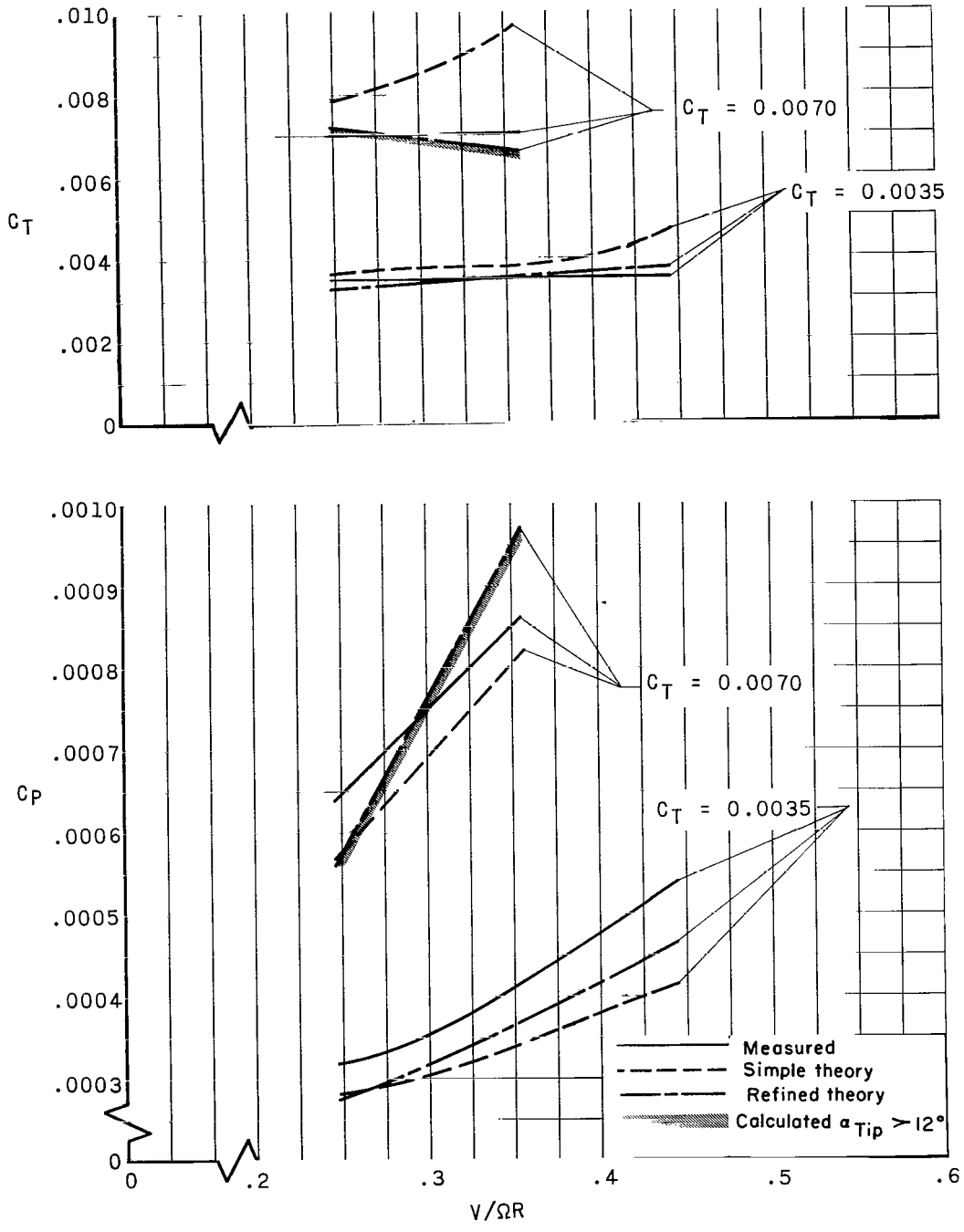

(a) Thrust and total-power coefficients.

Figure 14.- Comparison of measured and calculated rotor performance and flapping motions. Calculations are based on measured collective pitch and feathering motions. $\alpha_{TPP} = -9.5^{\circ}$.

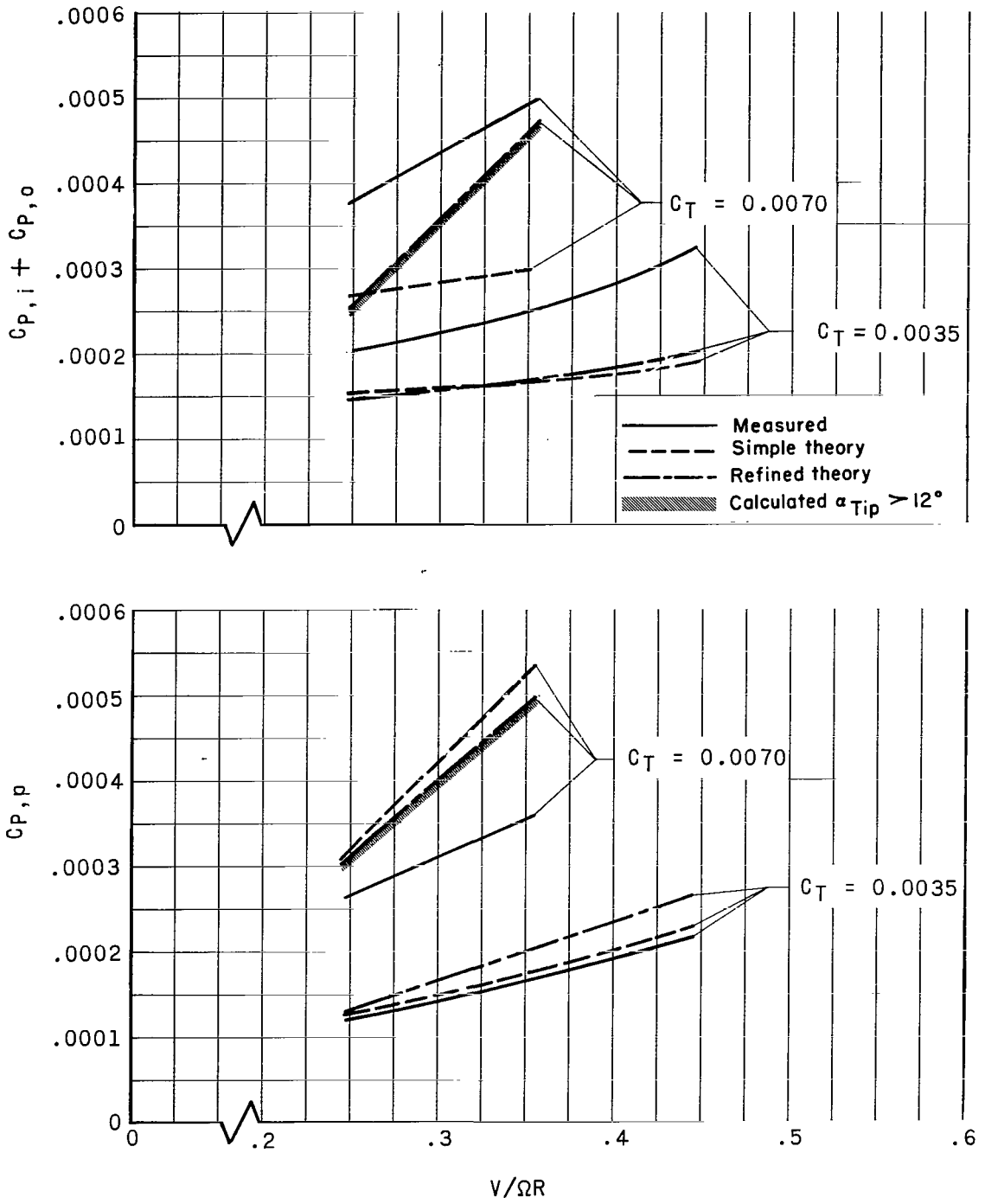

(b) Rotor-power and parasite-power coefficients.

Figure 14.- Continued.

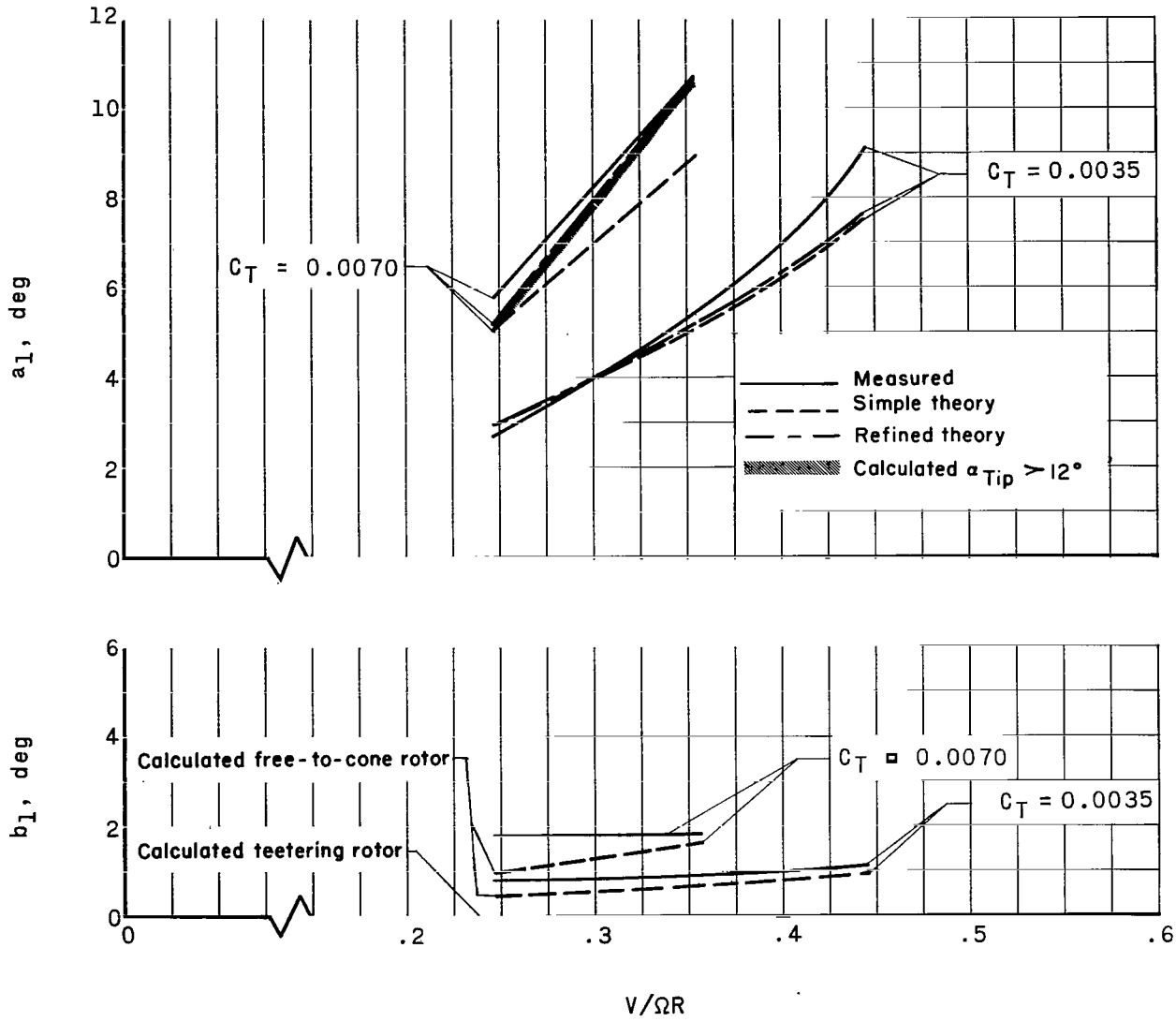

(c) Equivalent longitudinal and lateral flapping coefficients.

Figure 14.- Concluded.

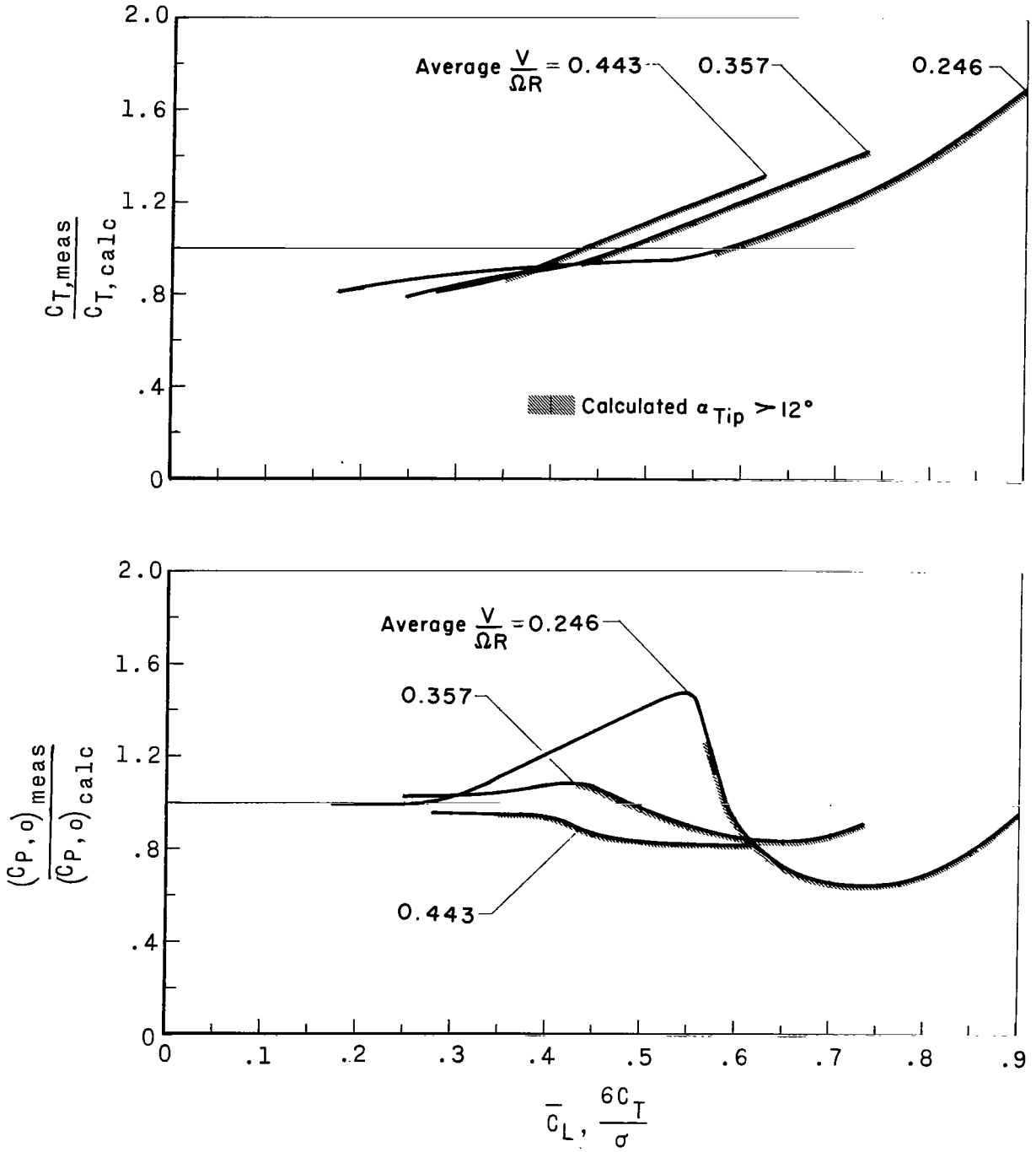

(a) $\alpha_{TPP} = 10.5°$.

Figure 15.- Variation of measured-to-calculated thrust and profile power ratios with equivalent hovering mean-lift coefficient. Calculations based on refined theory.

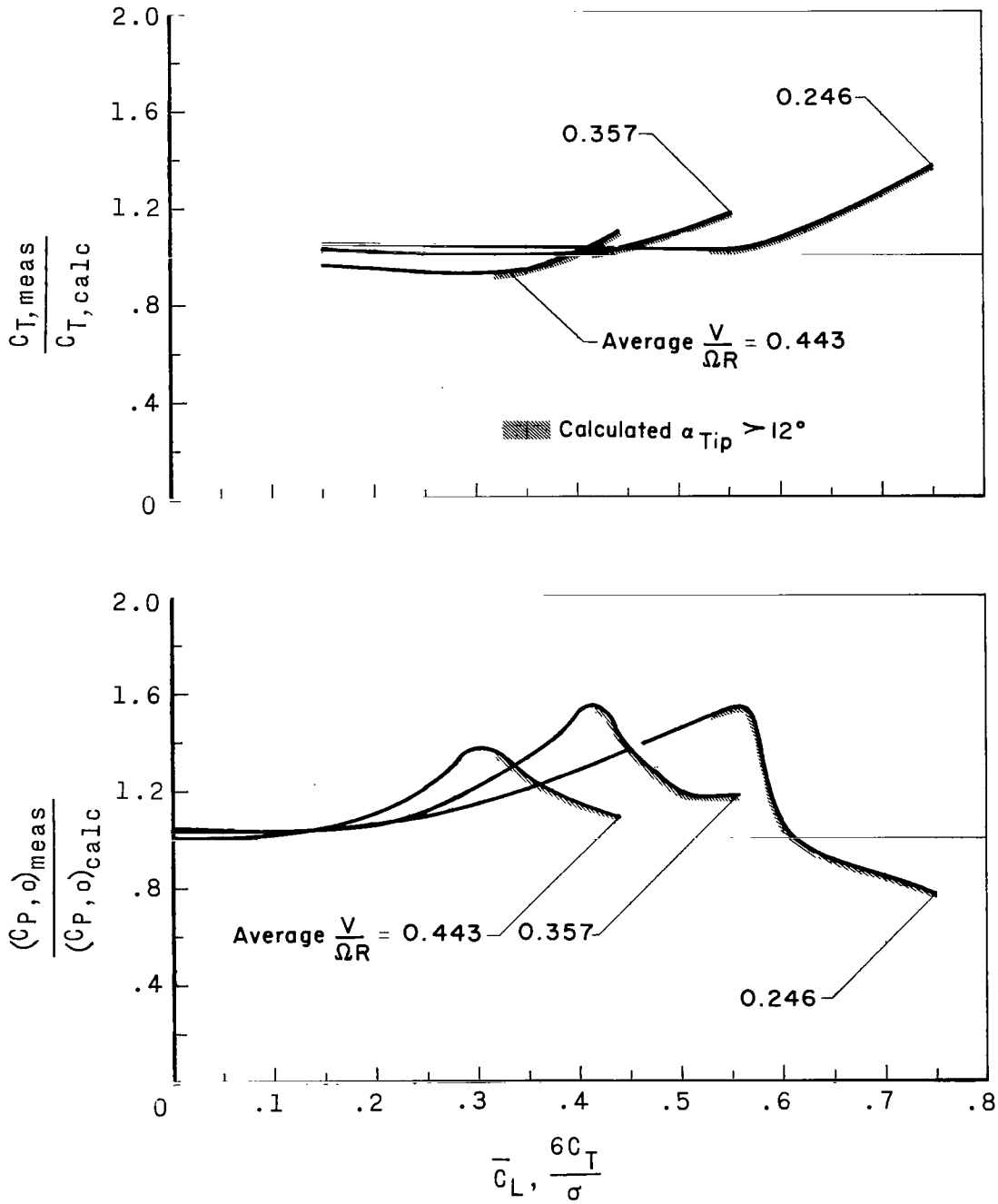

(b) $\alpha_{TPP} = 0.5°$.

Figure 15.- Continued.

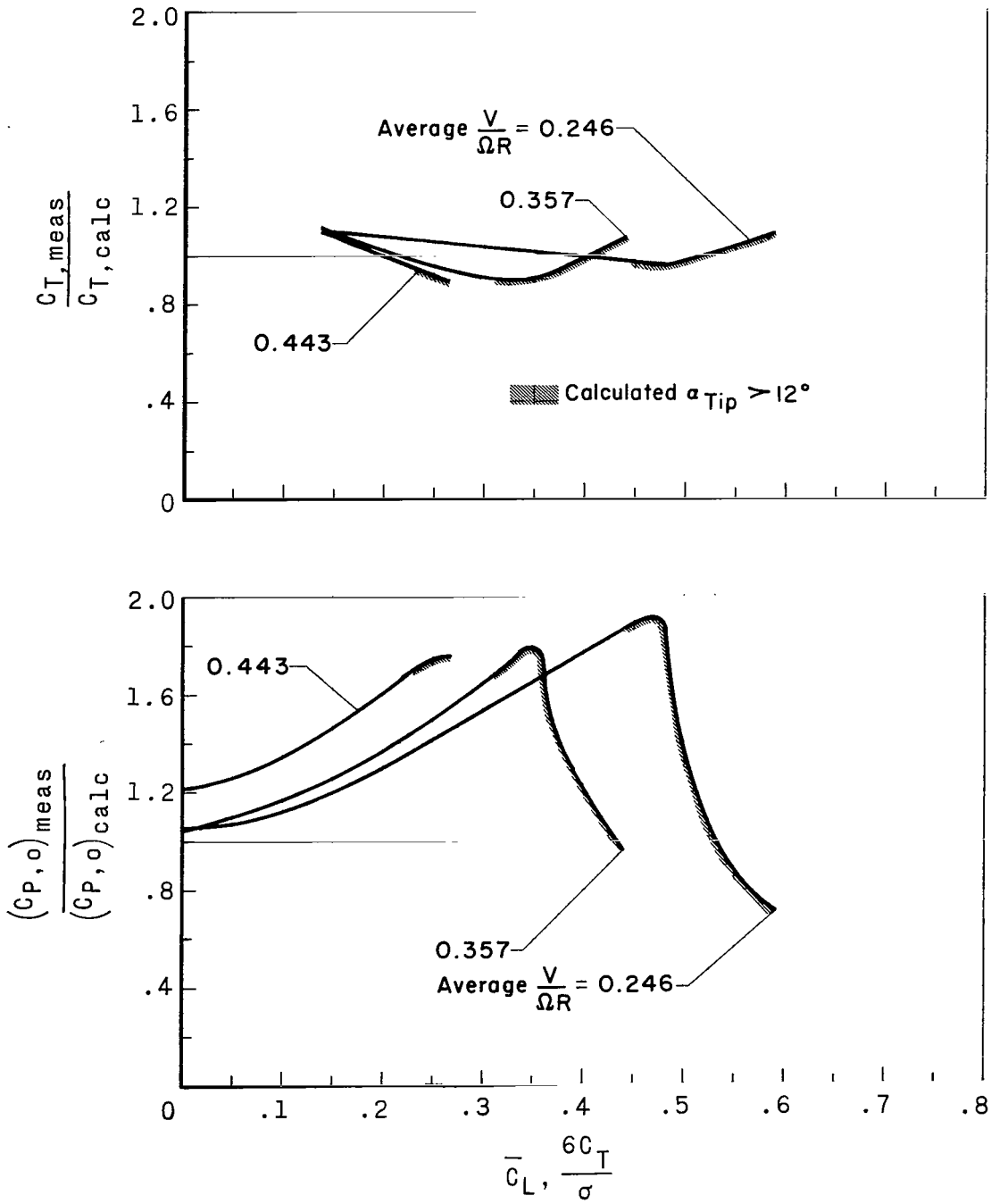

(c) $\alpha_{TPP} = -9.5°$.

Figure 15.- Concluded.

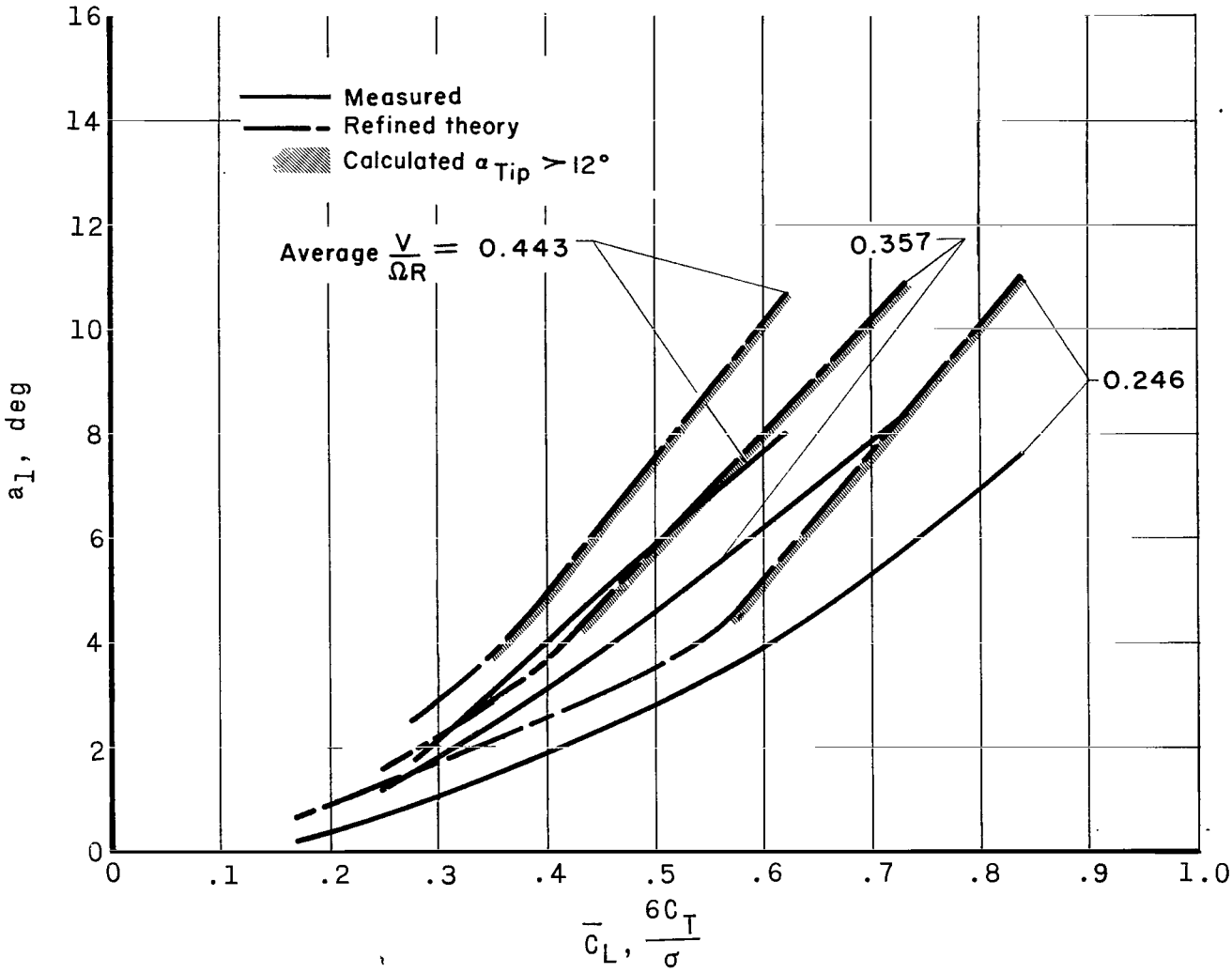

(a) $\alpha_{TPP} = 10.5°$.

Figure 16.- Variation of measured and calculated equivalent longitudinal flapping coefficients with equivalent hovering mean-lift coefficient.

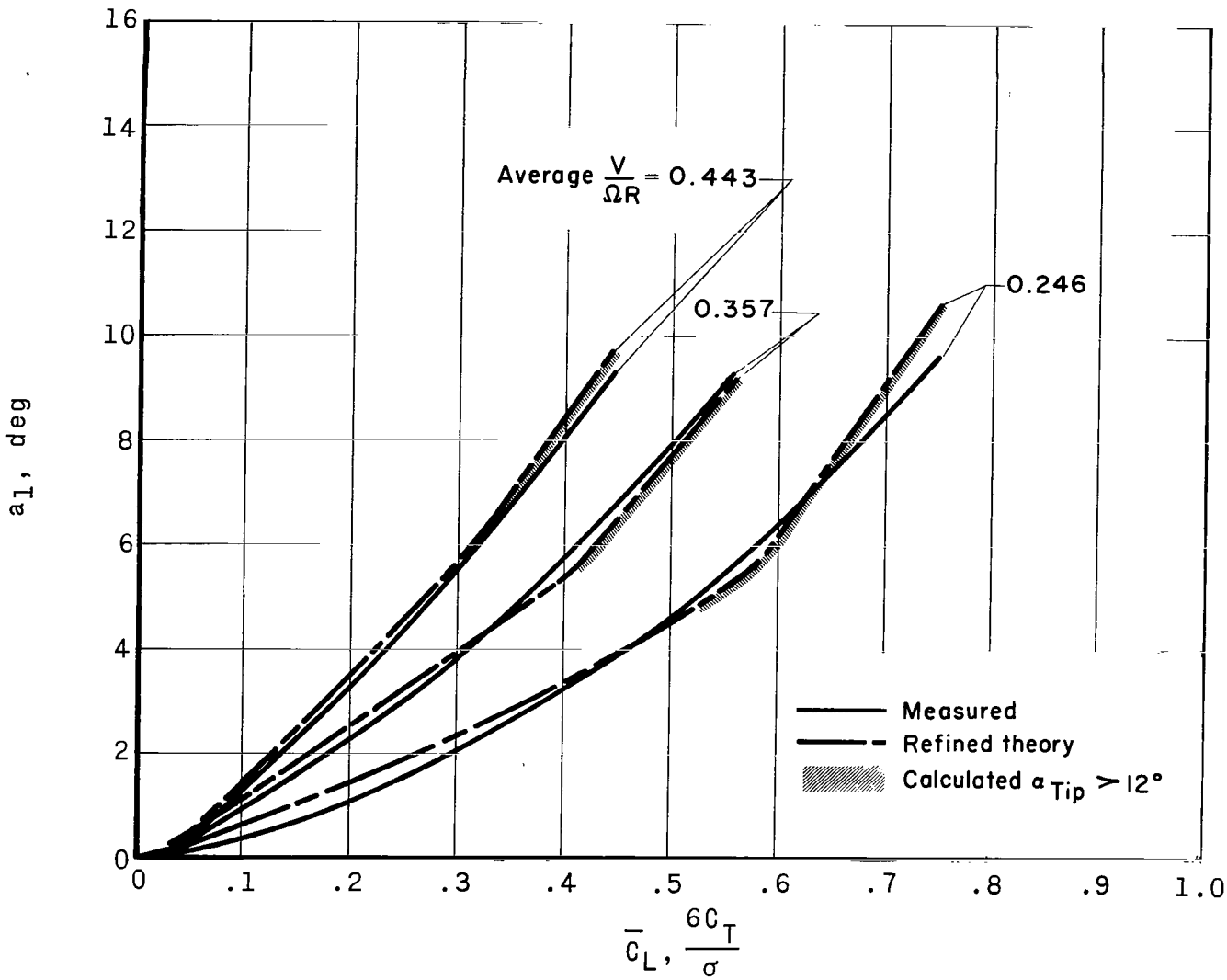

(b) $\alpha_{TPP} = 0.5°$.

Figure 16.- Continued.

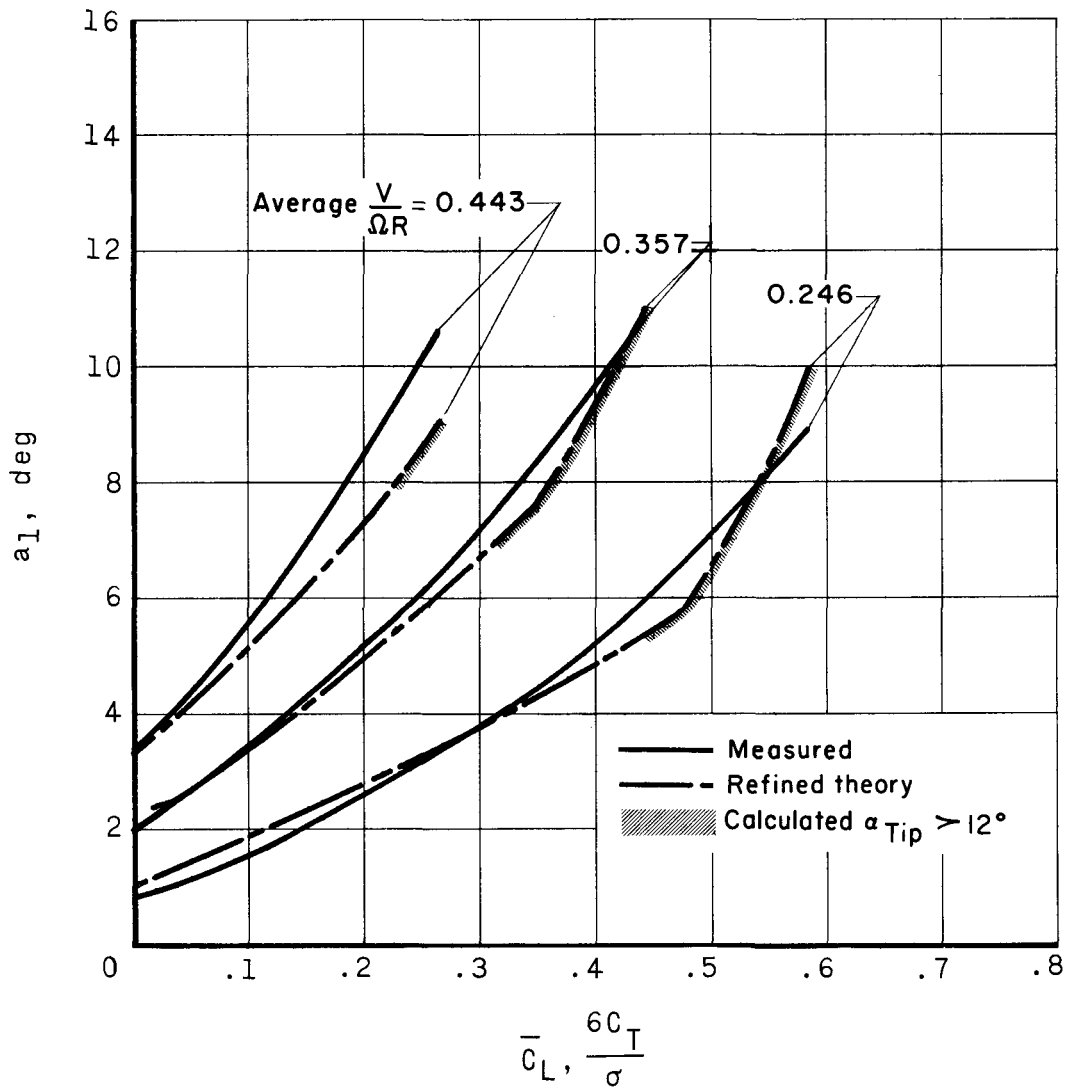

(c) $\alpha_{TPP} = -9.5°$.

Figure 16.- Concluded.

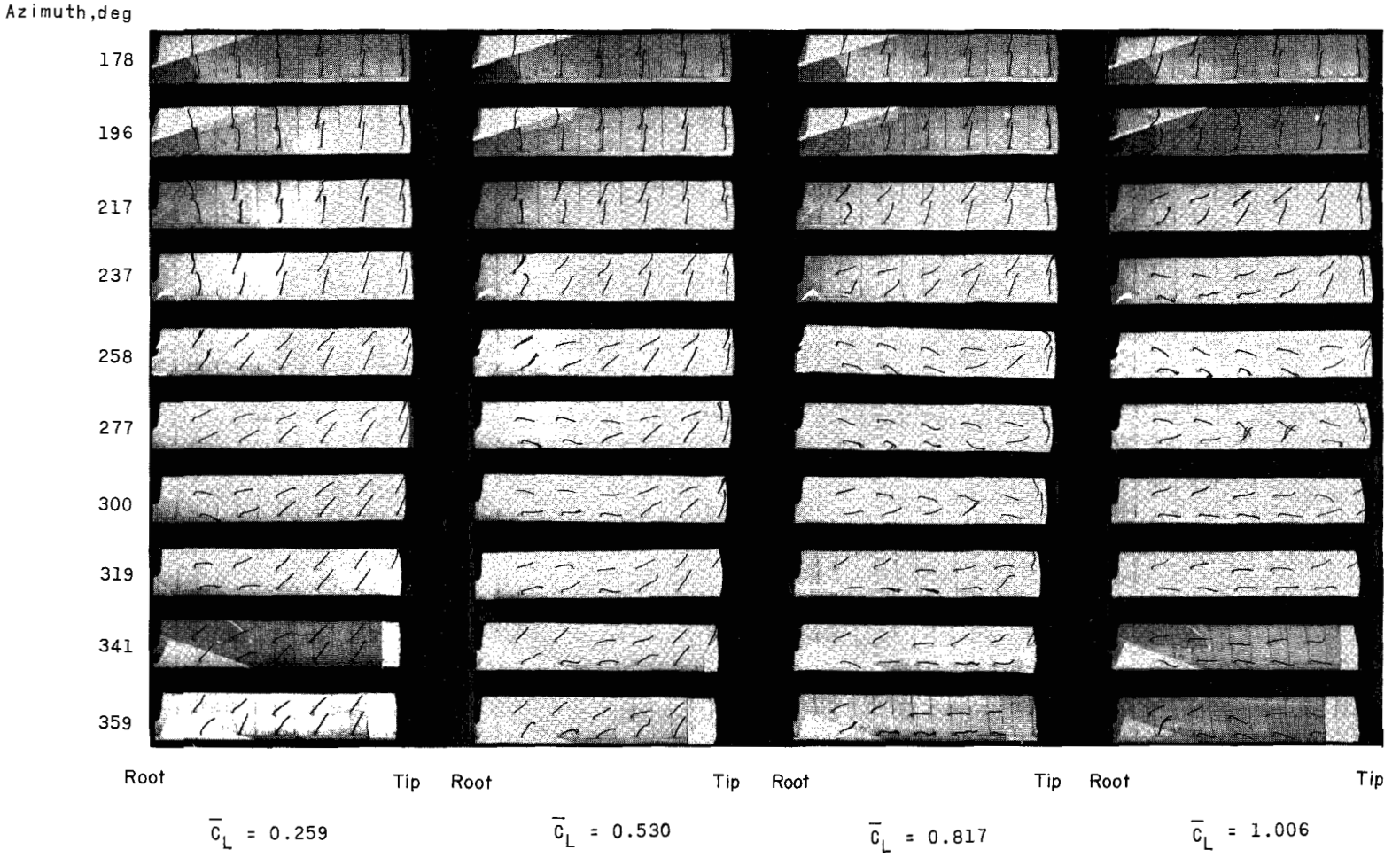

(a) $\alpha_{TPP} = 10.5^{\circ}$.

L-64-4713

Figure 17.- Variation of tuft flow patterns on the retreating side of the rotor disk with mean-lift coefficient (average $V/\Omega R = 0.246$).

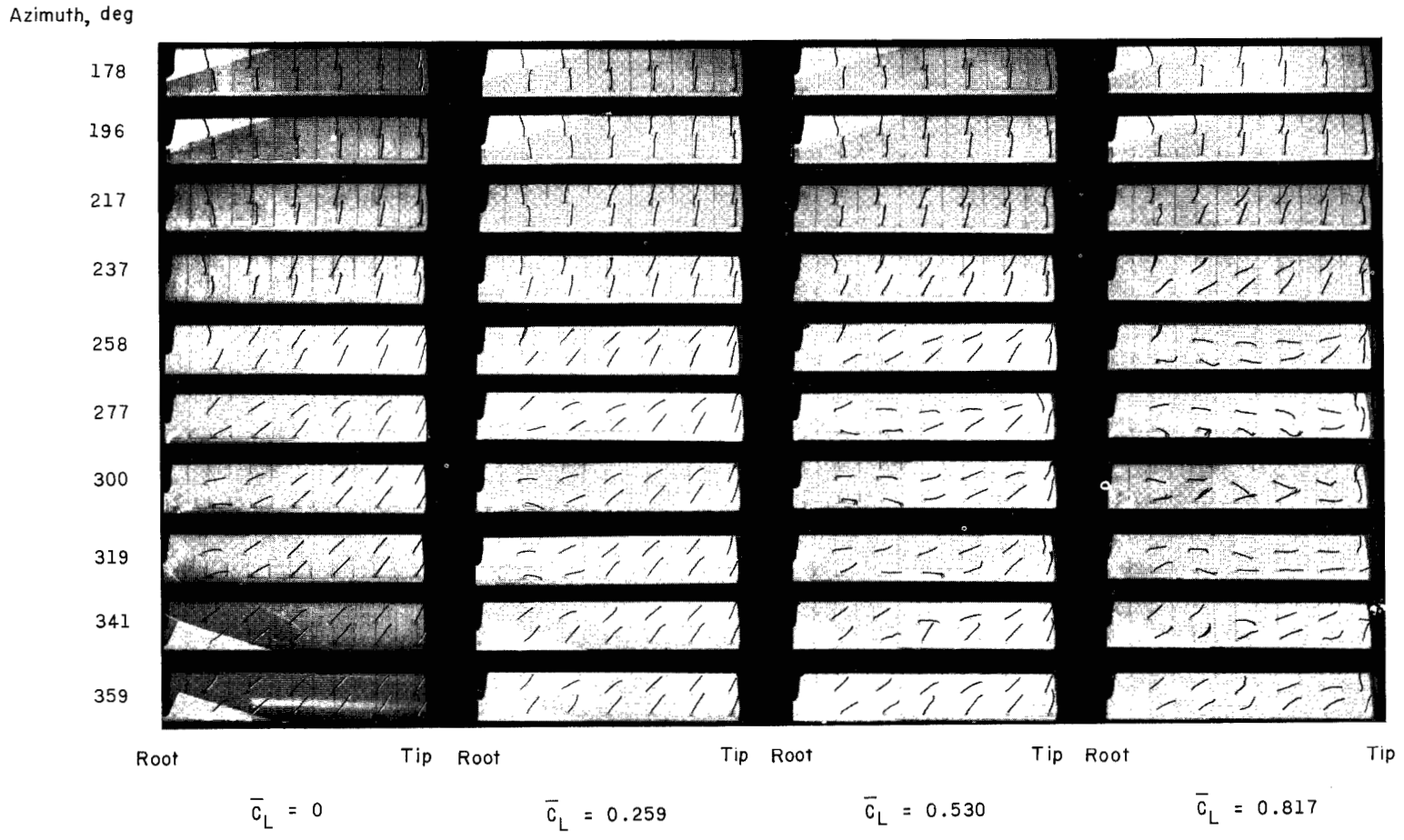

(b) $\alpha_{TPP} = 0.5^{\circ}$.

L-64-4714

Figure 17.- Continued.

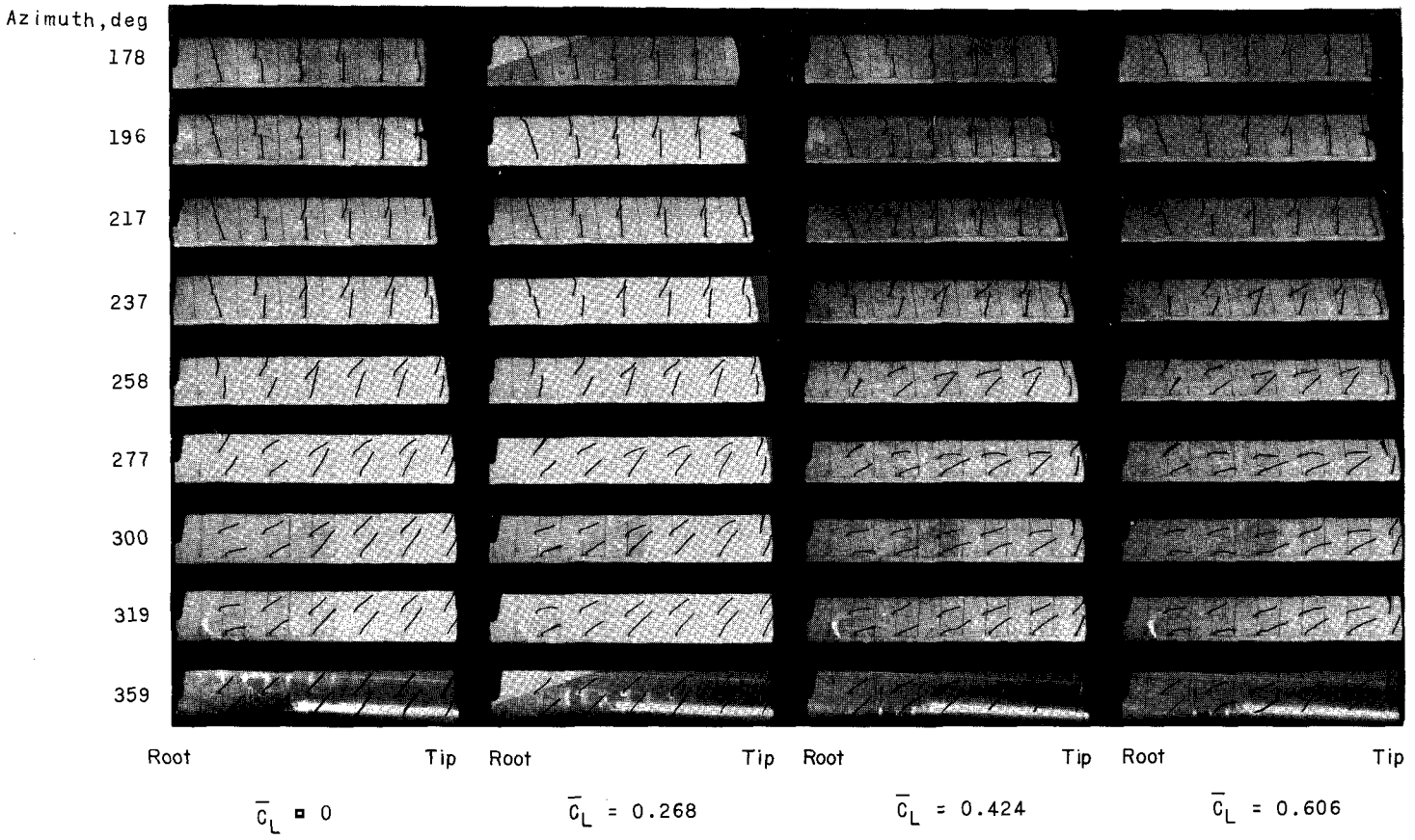

(c) $\alpha_{TPP} = -9.5^{\circ}$.

L-64-4715

Figure 17.- Concluded.

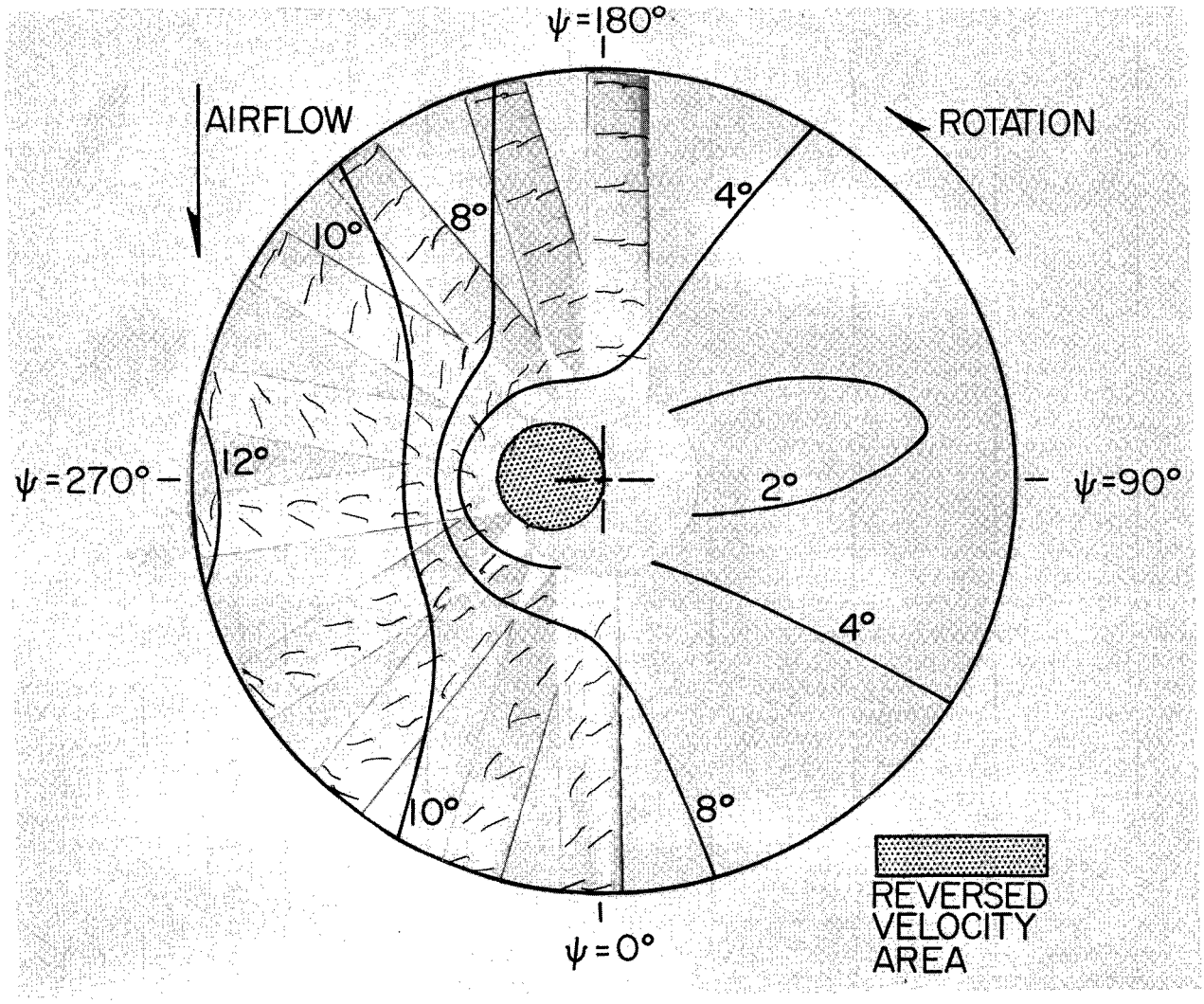

(a) $\bar{C}_L = 0.530$.

L-64-4716

Figure 18.- Comparison of tuft photographs with calculated contours of constant section angles of attack for a tip-path-plane angle of attack of 0.5°. $V/\Omega R = 0.246$.

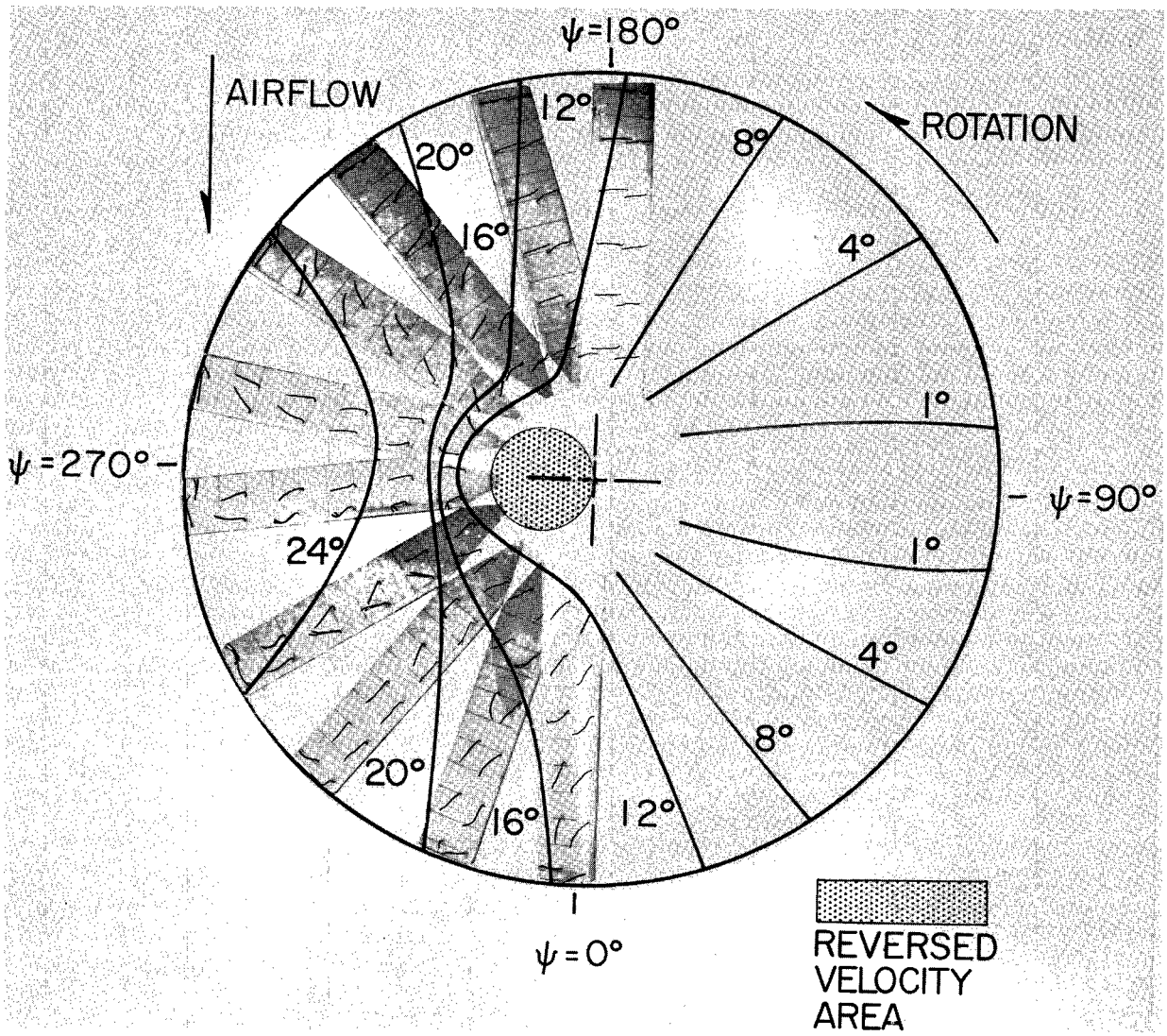

(b) $\bar{C}_L = 0.816$. L-64-4717

Figure 18.- Concluded.

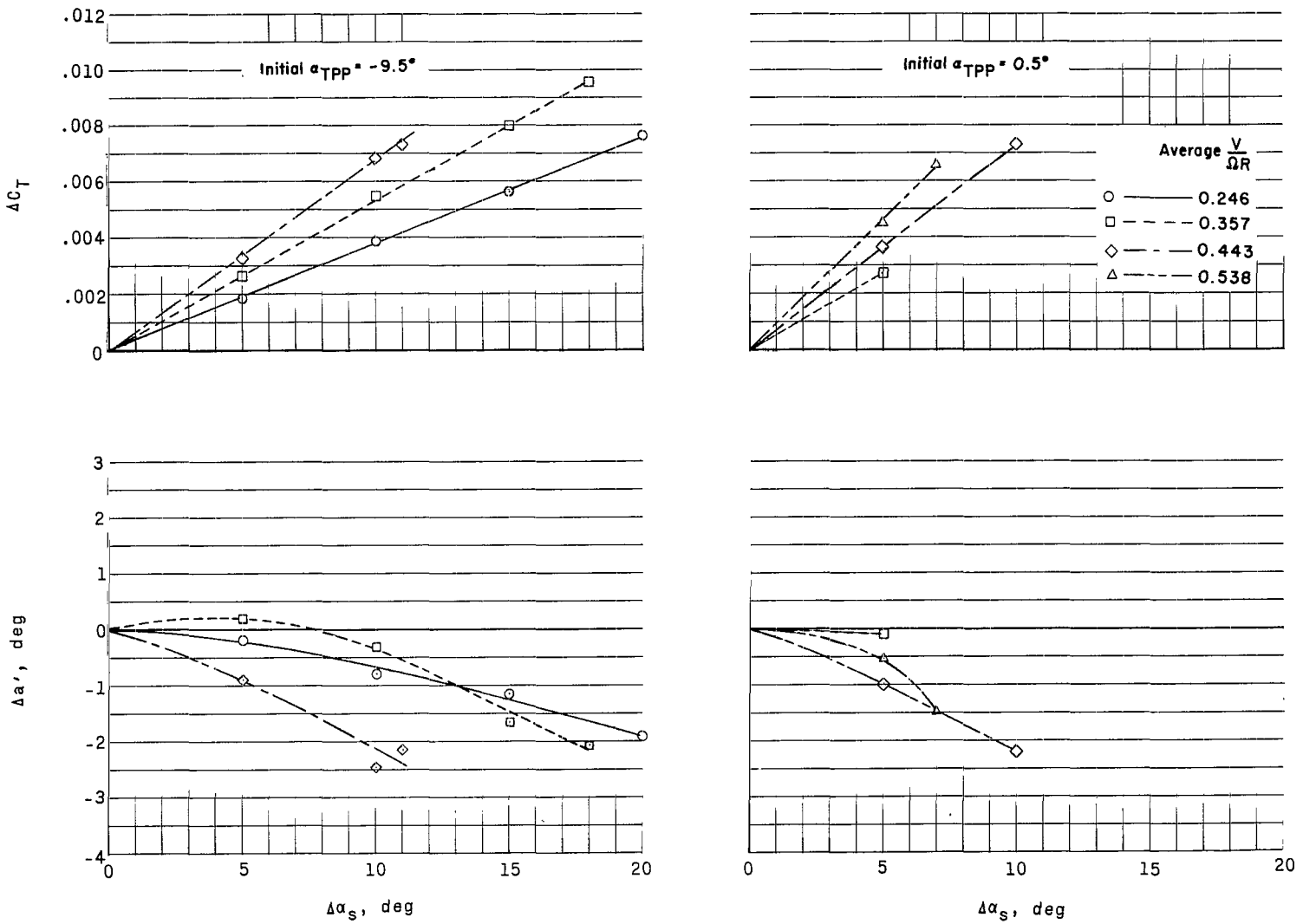

Figure 19.- Summary of rotor static stability measurements for large changes in shaft angle of attack. Average initial C_T = 0.0045.

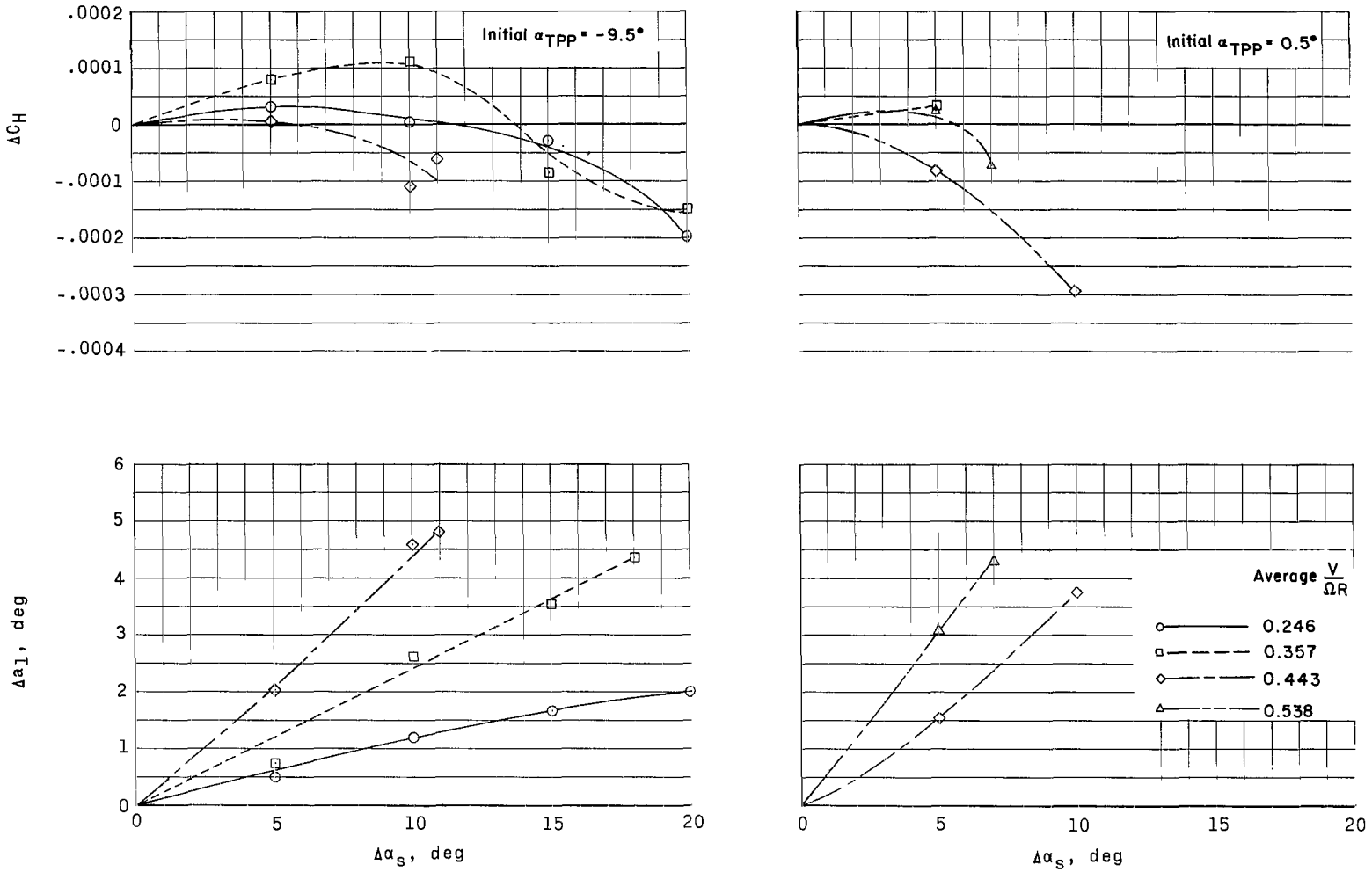

Figure 19.- Continued.

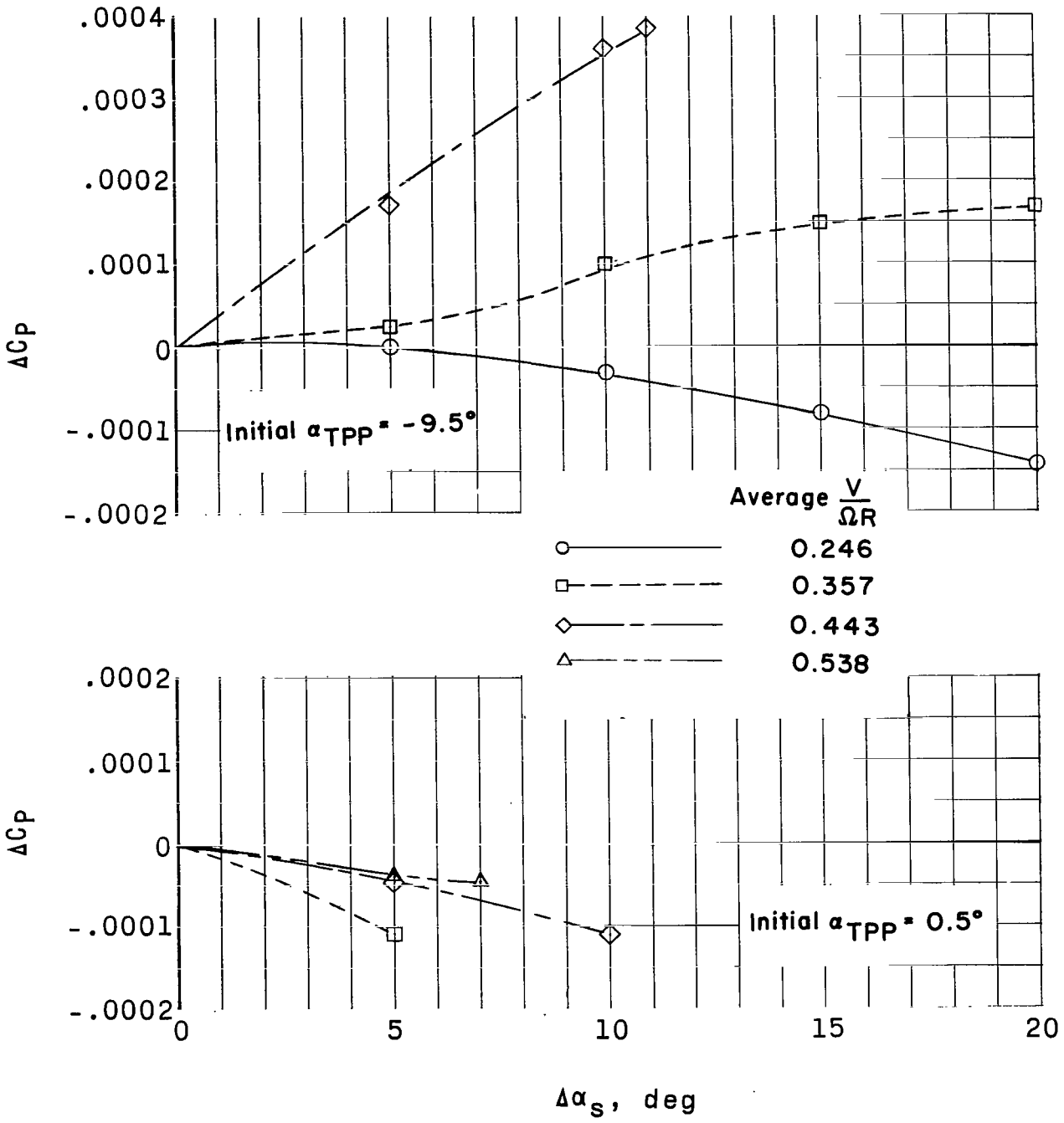

Figure 19.- Concluded.

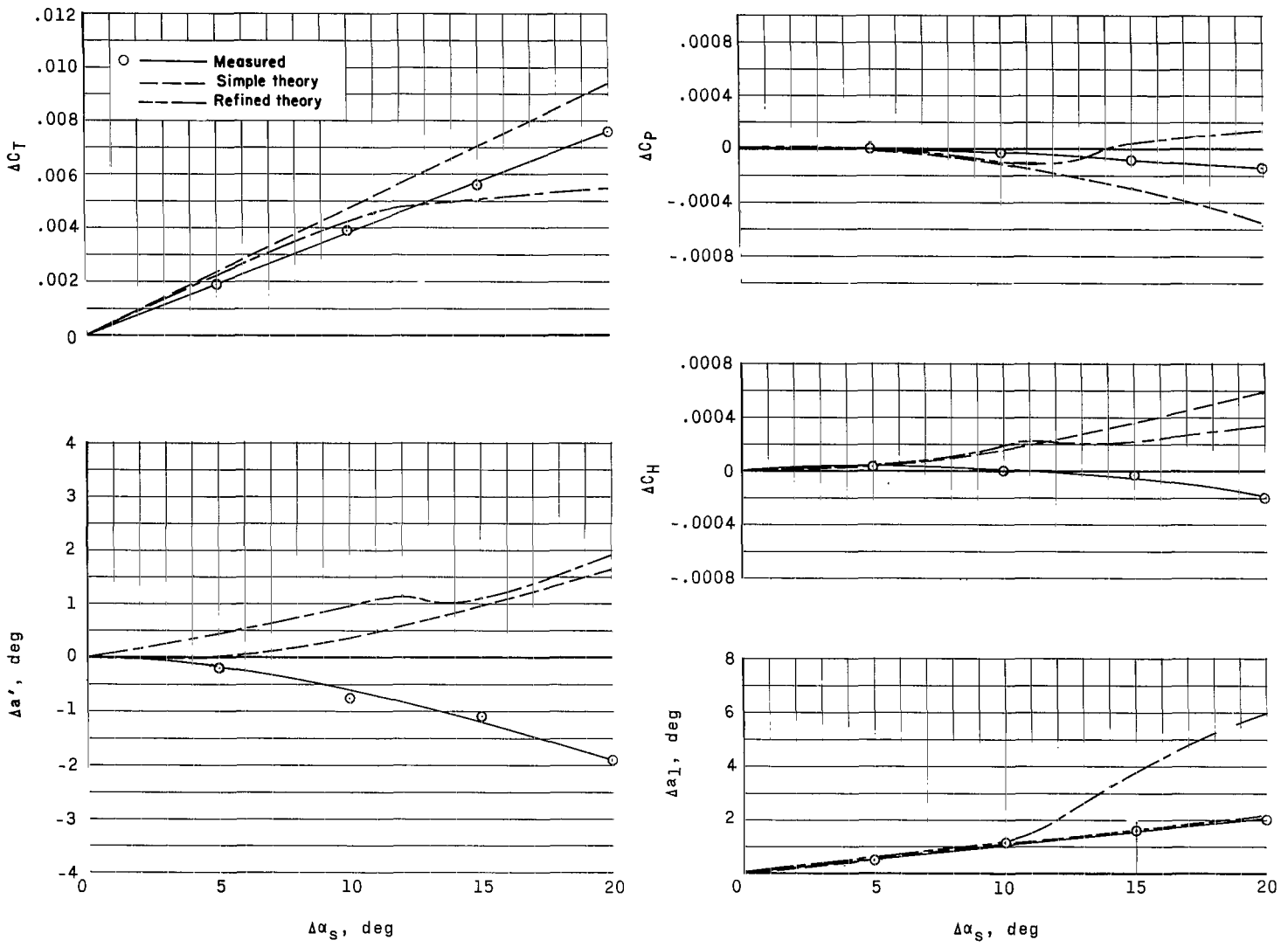

(a) Initial $C_T = 0.0045$.

Figure 20.- Comparison of changes in measured and calculated rotor static stability for large changes in shaft angle of attack. Initial $\alpha_{TPP} = -9.5^{\circ}$.

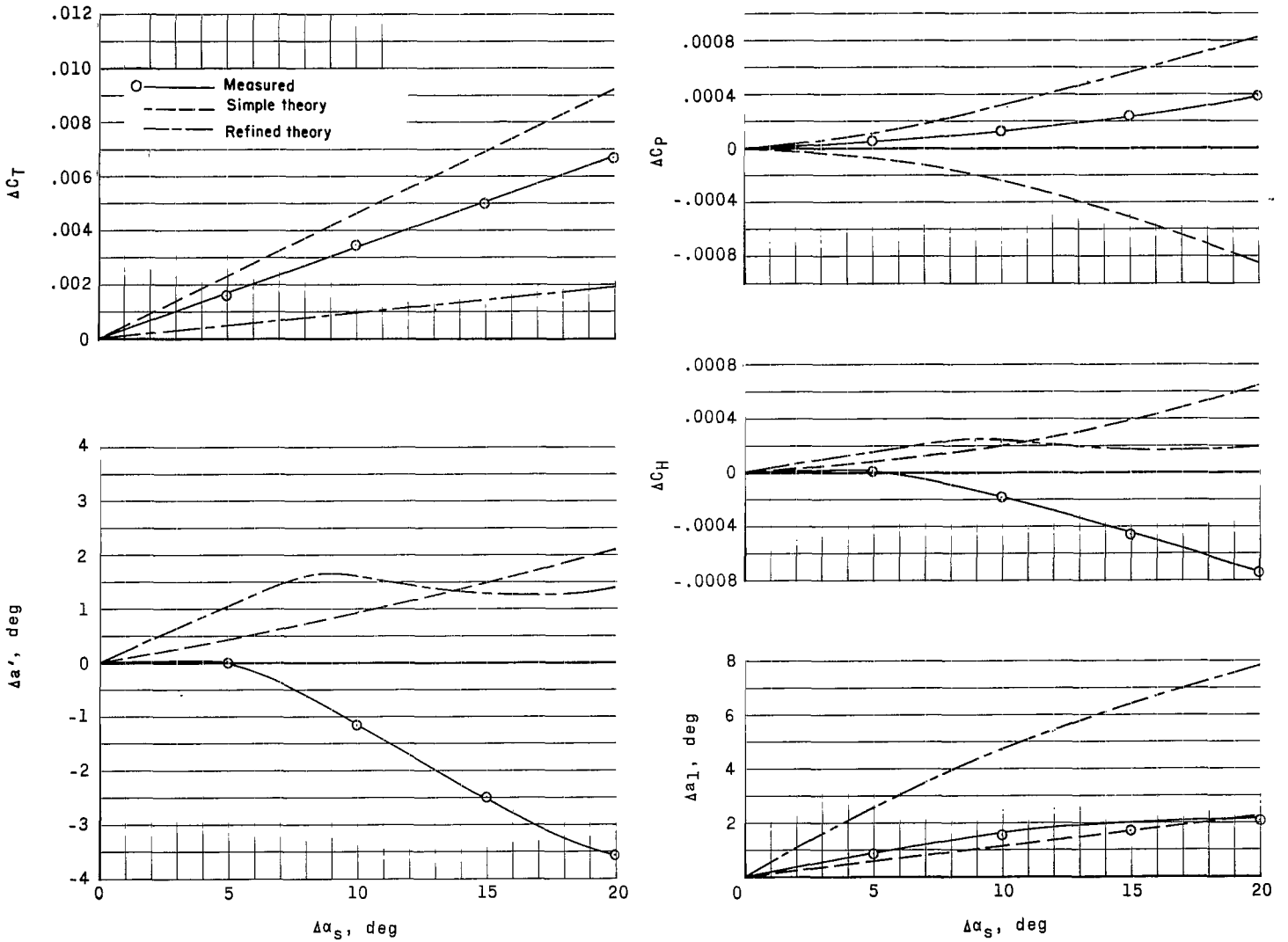

(b) Initial $C_T = 0.0090$.

Figure 20.- Concluded.

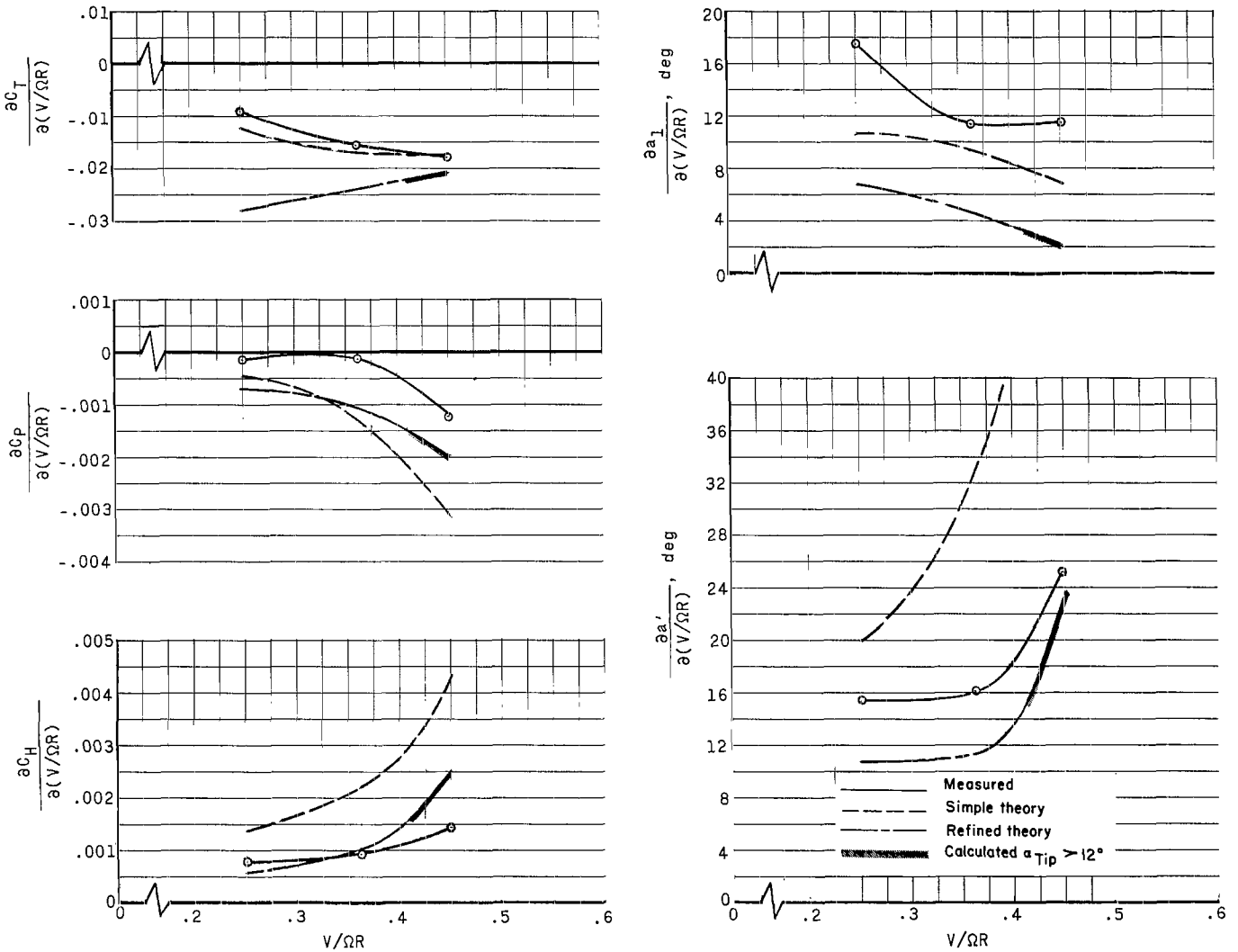

(a) Trim $\alpha_{TPP} = -9.5°$.

Figure 21.- Variation of speed-stability derivatives with tip-speed ratio. Average initial trim $C_T = 0.0045$.

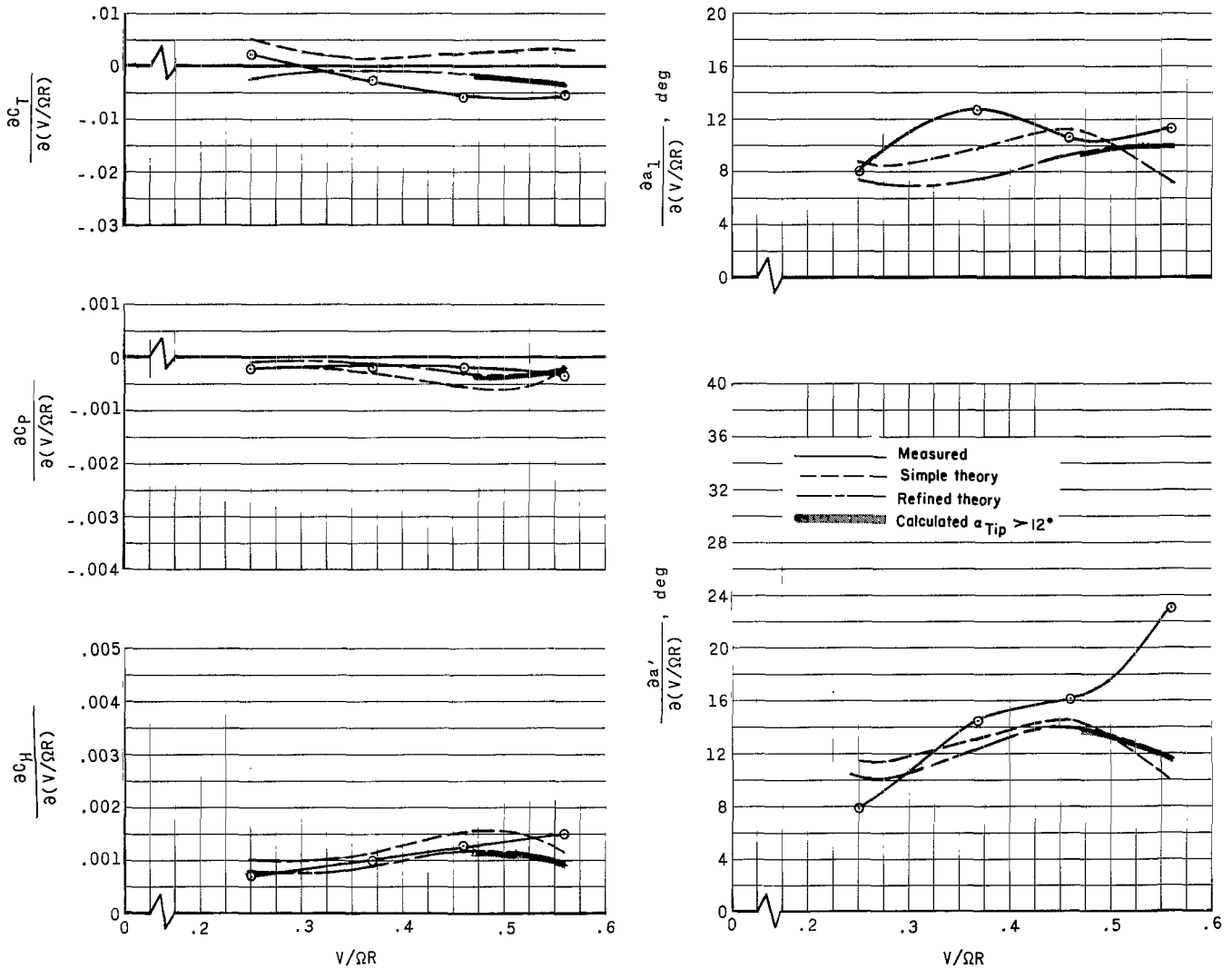

(b) Trim $\alpha_{TPP} = 0.5^{\circ}$.

Figure 21.- Continued.

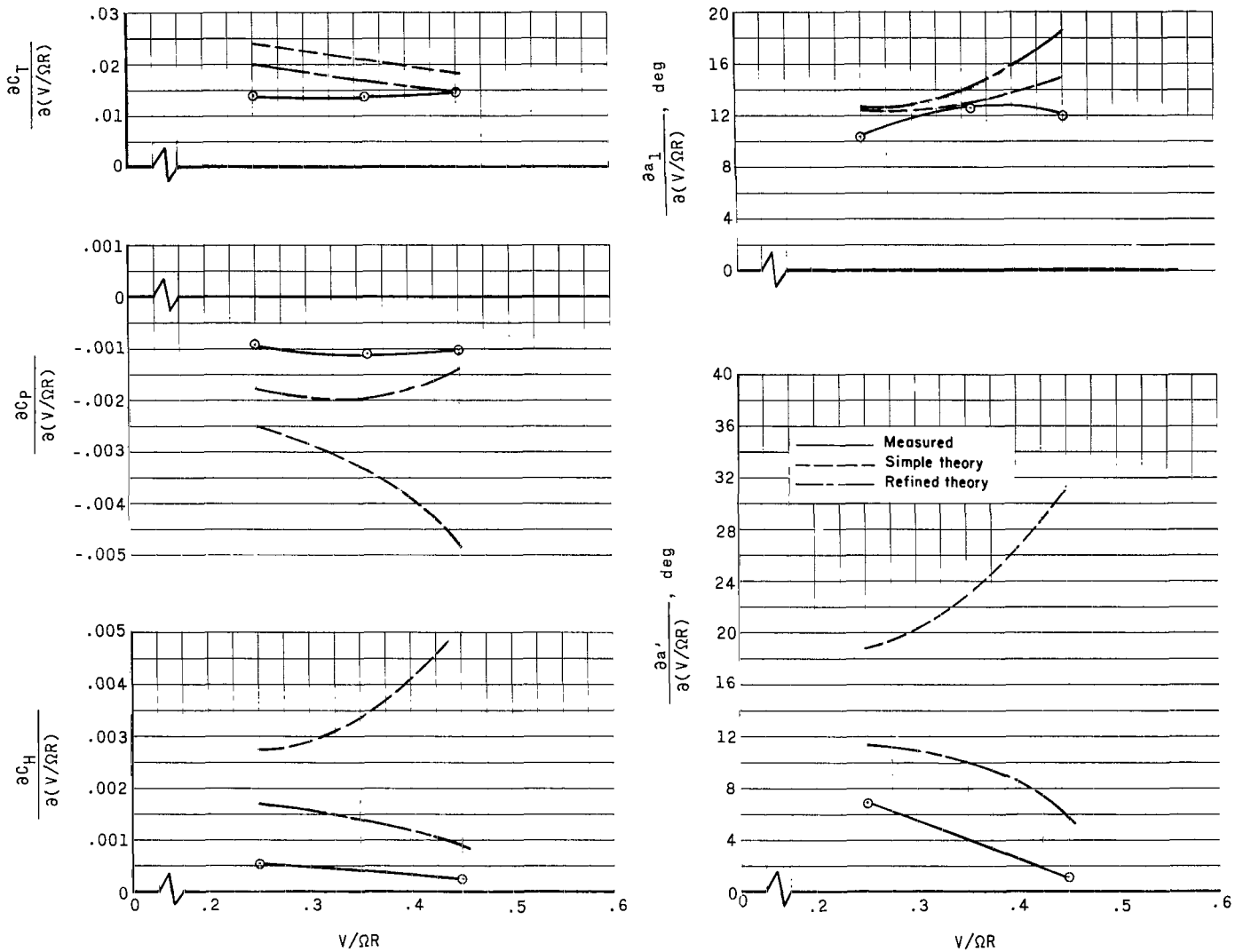

(c) Trim $\alpha_{TPP} = 10.5^{\circ}$.

Figure 21.- Concluded.

NASA-Langley, 1964 L-3896

2/7/85

"The aeronautical and space activities of the United States shall be conducted so as to contribute . . . to the expansion of human knowledge of phenomena in the atmosphere and space. The Administration shall provide for the widest practicable and appropriate dissemination of information concerning its activities and the results thereof."

—NATIONAL AERONAUTICS AND SPACE ACT OF 1958

NASA SCIENTIFIC AND TECHNICAL PUBLICATIONS

TECHNICAL REPORTS: Scientific and technical information considered important, complete, and a lasting contribution to existing knowledge.

TECHNICAL NOTES: Information less broad in scope but nevertheless of importance as a contribution to existing knowledge.

TECHNICAL MEMORANDUMS: Information receiving limited distribution because of preliminary data, security classification, or other reasons.

CONTRACTOR REPORTS: Technical information generated in connection with a NASA contract or grant and released under NASA auspices.

TECHNICAL TRANSLATIONS: Information published in a foreign language considered to merit NASA distribution in English.

TECHNICAL REPRINTS: Information derived from NASA activities and initially published in the form of journal articles.

SPECIAL PUBLICATIONS: Information derived from or of value to NASA activities but not necessarily reporting the results of individual NASA-programmed scientific efforts. Publications include conference proceedings, monographs, data compilations, handbooks, sourcebooks, and special bibliographies.

Details on the availability of these publications may be obtained from:

SCIENTIFIC AND TECHNICAL INFORMATION DIVISION

NATIONAL AERONAUTICS AND SPACE ADMINISTRATION

Washington, D.C. 20546